Photocopy and Use Authorization

In presenting this thesis in partial fulfillment of the requirements for an advanced degree at Idaho State University, I agree that the library shall make it freely available for inspection. I further state that permission for extensive copying of my thesis for scholarly purposes may be granted by the Dean of Graduate Studies, Dean of my academic division, or by the University Librarian. It is understood that any copying or publication of this thesis for financial gain shall not be allowed without my written permission.

Signature:____________________________

Date:_________________________________

TOPOGRAPHIC EVOLUTION AND SURFICIAL GEOLOGY OF REYNOLDS CREEK CRITICAL ZONE OBSERVATORY, SOUTHWEST IDAHO

by

Logan W. Mahoney

A thesis

submitted in partial fulfillment

of the requirements for the degree of

Master of Science in the Department of Geosciences

Idaho State University

Fall 2021

To the Graduate Faculty:

The members of the committee appointed to examine the thesis of LOGAN W. MAHONEY find it satisfactory and recommend that it be accepted.

Dr. Benjamin T. Crosby,
Major Advisor

Dr. Glenn D. Thackray,
Committee Member

Dr. Keith Reinhardt,
Graduate Faculty Representative

Acknowledgements

Throughout my journey as a master’s student, I have had a number of people that have helped me along the way that I would like to acknowledge. I would like to thank the Reynolds Creek Critical Zone Observatory (NSF Award # RGEO3E), the USGS EdMAP program, the GSA Student Research Grant, and the AGeS2 Grant program for supporting this project. I would not have been able to complete my project without the immense support I received from them.

Ben has been one of the most important mentors I have had in my life. Ben has never shied away from pushing me to be better, and always has been supportive and caring for my experiences at ISU. He may have been a busy person throughout my time here being the department chair, but I was always given the help whenever I needed, even if it meant being late to a meeting. I am forever grateful to have as wonderful of a mentor as Ben.

I would like to thank Dr Kathleen Lohse for her contributions with the NSF CZO funding, and for general guidance through my masters. I would also like to acknowledge the USDA-ARS crew, in particular Zane and Barry, for all their support in both land access and with any troubles I ran into while out in the field.

I would like to thank Utah State University for processing my OSL samples, even during a pandemic. I would also like to thank the Isotope Geology Laboratory at BSU for processing my U-Th-Pb samples during a pandemic. A big thanks to both Dr. Mark Schmitz and Dr. Corey Wells for providing insight and guidance to understanding my results.

I want to thank all the people who have offered time or resources during the development of this. Thank you to Dr. Jen Pierce and Dr. Virginia Gillerman for coming in the field to help explore Reynolds, to Dr. Barbara Nash for lending geochemical data to better understand the ashes present within the region, and to Dr. Glenn Thackray and Dr. Keith Reinhardt for willing to give feedback on the thesis document. I want to offer a special thanks to my field assistant, Josh Lingbloom, for joining me the entire summer, for being a wonderful bouncing board for ideas, and for putting up with my antics and constant bombardment of the Gus and Eddy podcast for the entire summer.

I would like to thank my peers and mentors at ISU for pushing me to become a better scientist. The skills you all have taught me will be immensely important.

Lastly, I would like to thank my partner during my time here, Holly Rucker. Though she may never have been in Idaho, she was always someone that I could trust, lean on, and get support even when I felt that I was unable to do something. She has pushed me to better myself as both a scientist and as a person, and I could not have asked for a better person to have in my life.

Table of Contents

List of Figures

List of Tables

Topographic Evolution and Surficial Geology of Reynolds Creek Critical Zone Observatory, Southwest Idaho

Thesis Abstract – Idaho State University (2021)

Geomorphic studies rarely focus on how the interplay of erosive and constructive processes can change the evolution of a landscape. Reynolds Creek, a 239 km^2 watershed, is used to study the interactions between constructive and erosive processes. The study was conducted using geomorphic mapping using LiDAR and field observations, geochronology, and topographic modelling. A lacustrine deposit, the Sedimentary Basin Fill of the Reynolds Basin area, reveals much of the topographic history of Reynolds Creek. The sediment was deposited after a rhyolitic flow dammed the watershed 11 Mya, filling the lower basin up with 150 meters of lacustrine and tuffaceous sediment. Dam incision followed fault motions related to the subsidence and formation of the western Snake River Plain. Breaching of the dam enabled incision of the basin fill, generating numerous river terraces. Reynolds Creek topographic evolution shares similarities to other volcanically dammed landscapes, but on a much larger scale. The disturbance still impacts the channel morphology 11 mya after the damming.

Keywords: Basins, Geomorphology, Surficial Geology, Topographic Evolution, Volcanic Damming

Chapter 1: Introduction

1.1 Motivation

The uplift and erosion of landscapes have been extensively explored over the past few years using numerical modeling (Tomkin, 2007, MacGregor et al., 2009) and geochemical techniques (Nasdala et al., 2002, Wintle and Murray, 2006). Geomorphic modeling often focuses on the transient response, a response to change in the system, following deviations from steady state, such as those that might occur after a change in erosional or constructional processes (refs). However, geomorphic modelling rarely focuses on constructional processes, such as volcanic deposition (e.g., Karlstrom et al., 2018). Reynolds Creek Experimental Watershed (RC), a 239 km^2 watershed in southwest Idaho (Figure 1.1), provides a natural laboratory for exploring how multiple depositional events can affect the topographic evolution of a watershed.

Groundwater was the primary research focus in Reynolds Creek at the inception of the USDA Agricultural Research Station (Robins, 1965). Groundwater research benefitted from understanding the bedrock geology of the region (e.g., McIntyre 1972). The current wave of active research in the watershed, supported by the National Science Foundation's program in Critical Zone Observatories, is more focused on the biogeochemical processes surrounding soil inorganic carbon (Seyfried et al., 2018; Flerchinger et al., 2019). This change of research emphasis would benefit from a surficial geologic map, which does not presently exist. A surficial geologic map would clarify the landform ages and processes that are directly affecting the soil, near-surface hydrology, and vegetation.

The goal of this project is to interpret the last 14 million year topographic evolution in Reynolds Creek based on field observations summarized within a 1:50,000 surficial geologic map. Our interpretations are supported by geochronologic data to constrain the volcanic depositional history of RC and to understand timing of stream incision and terrace abandonment. This also sheds light onto the evolution of the western Snake River Plain and the other watersheds flowing into that basin (Woods and Clemens, 2002; Beranek et al., 2006).

1.2 Background

1.2.1 Surficial Geologic Mapping

Surficial geologic mapping provides information on the surface sediments, their origin, and their properties. Surficial geologic maps differ from bedrock geologic maps as they focus on the thin skin of unconsolidated materials deposited over solid rock. Surficial geologic maps have a more contemporaneous correlation of map units (CoMU), as there are often numerous deposits forming at the same time. CoMUs of surficial geologic maps are also subdivided by the geomorphic processes that have been active in the region, generating fluvial, glacial, or colluvial deposits.

Data in surficial geologic maps is valuable to land management and development. Planning of land development is often based on safety requirements that use the data obtained from surficial geologic maps (Evans et al., 2009). Surficial geologic maps are also used for mineral exploration, in particular gravel and sand deposits used in construction (Moyle, 2004). Potential reservoirs of potable groundwater can also be assessed through the use of surficial geologic maps (Chase and Jeishampel, 2016).

High-resolution LiDAR, short for light detection and ranging, allows for finer detail interpretations to surficial geologic maps. LiDAR is a remote sensing technique used to measure high resolution (typically 1 meter spacing) elevations of the Earth's surface. LiDAR can measure the elevation through use of a laser. The laser shoots a pulse of light toward the earth, and is refracted back to a GPS receiver. The time it takes for the laser to reach the receiver records the elevation (Liu, 2008). This provides billions of x, y, and z coordinate that can be interpreted to create a digital elevation model (DEM). DEMs are derived into both digital terrain models (DTM) or digital surface model (DSM). These models differ as DSMs contain features on or above the ground surface, such as man-made material or trees, whereas DTMs only show the bare-earth surface. Geomorphic mapping largely uses DTMs. DEMs can be processed within programs such as ArcGIS Pro to produce derivative products, such as a shaded relief map or slope map (Haneberg, 2005). This processed data can be used to recognize landforms such as terraces or landslides within an area, even under dense tree cover.

1.2.2 Landscape Evolution

A landscape is a visible area of land and its landforms at a given point in time (King, 1983). Landscapes are continually progressing toward equilibrium in which the forces constructive and erosive processes balanced (Gilbert, 1877; Bracken and Wainwright, 2006). There are multiple types of equilibrium, describing specific situations that might occur (Bracken and Wainwright, 2006). At neutral equilibrium, a landscape does not change over time. This is unobtainable in natural landscapes. A dynamic equilibrium is an equilibrium that adjust to accommodate changes within a landscape (Gilbert, 1877). Landscapes can and often undergo disturbances that disrupt the evolutionary trajectory of a landscape. These disturbances change the state of a landscape, from either (1) equilibrium to a transient state or (2) transient state to a transient state (Mudd, 2016). These events are displayed in Figure 1.2. Following disturbance, the landscape experiences a reaction time, before the disturbance influences the overall landscape (Brunsden and Thomes, 1979). Reaction time is variable in duration, and depends on the type and location of the disturbance. The reaction time leads into a period of relaxation, where the landscape reacts to the disturbance and heads towards a new equilibrium (Bull, 1991). Landscapes do not need to reach a new equilibrium before experiencing another disturbance.

Landscapes are shaped by two domains of processes: constructional and erosional. Constructional processes occur through deposition of material, rock uplift, or surface uplift in a landscape to change the topographic form of the landscape (Hughes, 2010). Constructional processes can create closed depositional basins. The formations of a closed depositional basin must have a constricted exit, whether that be from damming from some sort of blockage (landslide, volcanic, etc.) or through tectonic movement.

Erosion causes the breakdown and removal of material from a landscape via hillslope, fluvial and glacial processes (Hughes, 2010). Erosional processes often dominate studies of landscape evolution.

1.2.3 Geomorphic Landforms

Landforms are natural features on the Earth’s surface. Two key landforms in RC are river terraces and knickpoints. These landforms are present within the lower basin, and are used to interpret the later history of RC.

1.2.3.1 Terraces

River terraces record past stream incision and abandonment of fluvial surfaces through time (Pazzaglia, 2013). Terraces are low relief surface that appears near a stream. They are comprised of a bounding steeper side called a riser, and flat gently sloping plain called a tread. The terraces can come in pairs and can be identified based on their elevation from the stream, but can also be unpaired. Terraces tend to have a steeper slope on the side that is closer to the stream. River terraces differ from floodplains as they lie high enough above the stream channel to not be influenced by flooding events (Pazzaglia, 2013; Yan et al., 2017). Terraces are created through the process of lateral planation, followed by vertical incision (Hancock and Anderson, 2002). Terraces treads can be formed in two distinct ways, by strath planation or by alluvial fill.

Strath terraces are formed through downcutting of a stream into bedrock with little to no alluvial fill (Pazzaglia, 2013). The bedrock in this case can be any substrate that is present beneath the stream. Strath terraces begin formation with lateral planation of the stream bed (Hancock and Anderson, 2002; Schanz et al., 2019). Alluvial fill is not thick on the planed surface. The stream then incises into the channel, abandoning the old stream bed and creating a strath terrace. Strath terrace formation results from tectonic influences, and has a longer response time due to needing more force to overcome the baselevel change (Schanz et al., 2018). Strath terraces can sometimes be confused for alluvial terraces if the substrate of the bedrock is poorly consolidated to unconsolidated material (Finnegan and Dietrich, 2011; Finnegan and Balco, 2013; Pazzaglia, 2013).

Alluvial fill terrace formation begins with valley filling by alluvial deposits transported (Pazzaglia, 2013). Subsequent incision cuts back into the fill, leaving behind the abandoned fluvial surface (Hancock and Anderson, 2002). Alluvial fill terraces are largely susceptible to changes in climate or tectonics as these factors influence sediment aggradation and evacuation (Merrits et al., 1994; Bestland 1997, Tofelde et al., 2019).

Terraces can be used to reconstruct the incision and aggradation history of a stream (Briant et al., 2012). Terrace geometry can be visualized above a long profile of the current stream. With the use of optically stimulated luminescence data, researchers can recreate the overall incision history of a region. An assumption can be made that alluvial material was continuously reworked until incision occur, isolating the terrace from active fluvial processes, resulting in the final deposition of the material.

1.2.3.2 Knickpoints

Knickpoints or knickzones are areas within a channel where there is an abrupt change in elevation relative to upstream or downstream reaches. Knickpoints are usually expressed as waterfalls in the micro scale landscape. In the macro scale, knickpoints are expressed as areas of anomalously steep channel beds that can extend for tens of kilometers (Crosby and Whipple, 2006). These knickpoints are indicative of either (1) changes in the base level from a downstream disturbance or (2) contrasting lithology within stable landscapes. Knickpoints can be an erosional front that represents the change between the relict and the disturbed landscape (Crosby and Whipple, 2006; Harkins et al., 2007; Lague, 2013). The changes in the base level can be on a small scale, such as landslide damming, or large scale, such as fault growth or throw, which creates an incision signal which propagates upstream forming the knickpoints (Whipple and Tucker, 1999; Crosby and Whipple, 2006; Cook et al., 2013). For stable landscapes, contrasting lithology can create knickpoints. Resistant material located between erodible material can create knickpoints, as the resistant material can retain steeper slopes.

Knickpoints can provide useful information to reconstruct the history of a stream channel. Through the use of terrace reconstruction, an inference can be made that correlates the abandonment and incision of a river terrace with the upstream translation of a knickpoint to determine if the relict stream was in a consistent location before or after the disturbance event occurred (Finnegan, 2013). Determining the rate of incision for a given knickpoint can also be used to reconstruct the location and cause of the knickpoint creation (Berlin and Anderson, 2007; Whittaker and Boulton, 2012).

1.2.4 Geochronology

1.2.4.1 U-Th-Pb Dating

U-Th-Pb geochronology is a dating technique that provides a crystallization age for specific minerals, most common being zircon. The determination of this date is based on the decay of three parent isotopes: ^{238}U, ^{235}U, and ^{232}Th (Schoene, 2014). All three of these isotopes undergo alpha decay, where in the nucleus emits an alpha particle of helium which reduces the atomic mass by four and the atomic number by two, until producing a daughter isotope product (Lee et al., 1997). The daughter isotopes in this radioisotope system are ^{206}Pb for ^{238}U, ^{207}Pb for ^{235}U and ^{208}Pb for ^{232}Th (Romer, 2013). This data is plotted on a concordia diagram, which plots the ratio of known values of $^{207}Pb/^{235}U$ vs $^{206}Pb/^{238}U$ that is used for comparison against experimental data (Harley and Kelly, 2007). The experimental data is cross referenced with error bars to accurately define the age of the zircons.

This dating technique is used to help determine timing of volcanic events, metamorphic events, provenance analysis, and for structural geologic analysis. The dating of volcanic events with U-Th-Pb geochronology requires determining if the grains are from primary ash fall deposits and have not been reworked (Rasmussen and Fletcher, 2010; Rocha-Campos et al., 2011). This determination can be done on large populations of zircon grains through the use of laser-ablation inductively coupled plasma mass spectrometry (LA-ICP-MS). Primary grains can undergo chemical abrasion isotope dilution thermal ionization mass spectrometry (CA-ID-TIMS) for more precise ages. For provenance analysis, the grains must be detrital in nature and based on the peaks can be associated with larger geologic events revealing the source and transport history of the grains (Beranek et al., 2006). For structural analysis, correlating beds with similar U-Th-Pb dates can be used to determine onset movement of faults (Wang, 2005).

1.2.4.2 OSL Dating

Optically Stimulated Luminescence (OSL) is a dating technique that determines when a grain of sediment was last exposed to sunlight (Lian, 2007). The technique determines this time by measuring the amount of radioactive decay absorbed from the surrounding environment. Sediment that is buried slowly excites electrons that are being produced from the surrounding environment (Rhodes, 2011). These electrons are trapped within breaks in the lattice, commonly found in grains such as quartz or feldspar (Aitken, 1998). The timing of burial can be reset if either 1) the sediment is heated to a high enough temperature (500 °C) or through exposure to sufficient sunlight. This occurs because it reduces the luminescence signal to a low residual level.

The age calculation requires two measurements: an accumulated dose and a dose rate. The accumulated dose is a measurement of the total amount of accumulated energy per unit mass of a sample since the hypothetical resetting event. This is determined through the use of single-aliquot regenerative method to determine a dose equivalent (Murray et al., 2000). The method involves creating regenerative doses that are plotted on a curve, and finding the intercept of that natural luminescence signal with the regenerative doses signal. The dose rate is the rate at which this energy is accumulated. This is determined through the use of dosimeters and/or sample collecting adjacent to the dose equivalent sample and analyzed with ICP or other methods (Murray et al., 2000).

OSL is particularly useful in understanding timing of abandonment of fluvial terraces. The grains present within an active riverbed are continuously being reworked and exposed to the sun during transport. Once the abandoned through incision, deposition ceases, capturing abandonment age of the terrace (Geach et al., 2015; Olszak et al., 2016; Berndt et al., 2018).

1.3 Study Area

1.3.1 Historical Background

Interest in RC geology began in 1904 by Lindgren and Drake focusing on ore deposits. The area would remain largely unstudied until 1965, when the Agricultural Research Service established RC with research interest on groundwater movement (Robins et al., 1965). David H. McIntyre created the first large scale geologic map of Reynolds Creek in the late 1960s, with updates done in 1981 by Ekren and 2006 by Bonnichsen and Godchaux. These updated maps were created at larger scales, and added in geochronologic constraints units, such as an Ar-Ar date of the Rhyolitic lava flow of Reynolds Creek (Bonnichsen et al., 2004). In 2015, Reynolds Creek was established as a critical zone observatory, with the focus of study changing from groundwater towards biogeochemical processes within soil (Lohse et al., 2015).

1.4 Problem Statement

Landscapes that undergo damming events experience major changes in its topographic evolution. These landscapes follow a process of damming, then fill, then spillover, then incision to evolve over time, but do not leave behind signals for this transition that last more than one million years (get sources from Ch. 3). RC provides an environment to determine if signals of damming are present past the one million year marker. Determining if these signals exist are based on examining the topographic profile and the surficial landforms, such as river terraces, landslides, knickpoints, and volcanic deposits, throughout RC. Understanding the location of river terraces and knickpoints can be used to reconstruct how the stream has migrated (Litchfield and Berryman, 2005; Briant et al., 2012; Viveen et al.; 2013) and how disturbances appeared and propagated through the streams (Crosby and Whipple, 2006; Cook et al., 2013), while defining the extent of the volcanic deposits can help reconstruct the pre-erosional landscape (Thouret 1999). This information combined with analysis of the topographic profile can be used to determine what signals were left by the damming events.

The geomorphic and geologic history of RC is poorly constrained. In particular, the sedimentary basin fill of RC has no geochronologic ages associated with it. The sedimentary basin fill of RC is the key to unravelling and interpreting the geomorphic history of RC.

I use high resolution LiDAR to map out the surficial landforms present within RC in order to interpret the sequence of events for the evolution caused by the damming event were derived. I further define the timing of events through the use of U-Th-Pb techniques on primary ash fall tuffs and Optically Stimulated Luminescence techniques on sand lenses within river terraces.

1.5 Figures

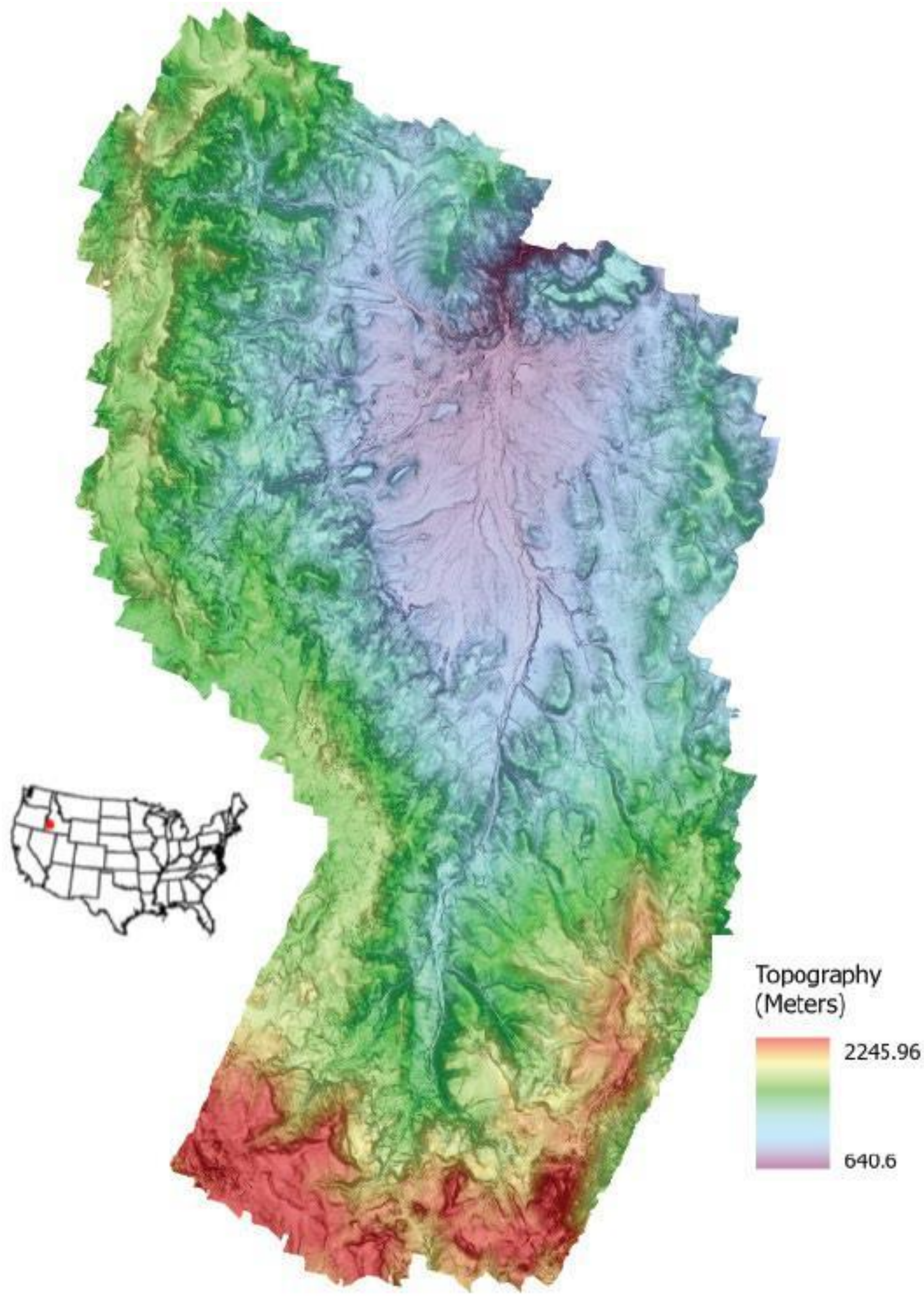

Figure 1.1: DEM of Reynolds Creek, Idaho. US map to the left marks the location of Reynolds Creek with a red dot.

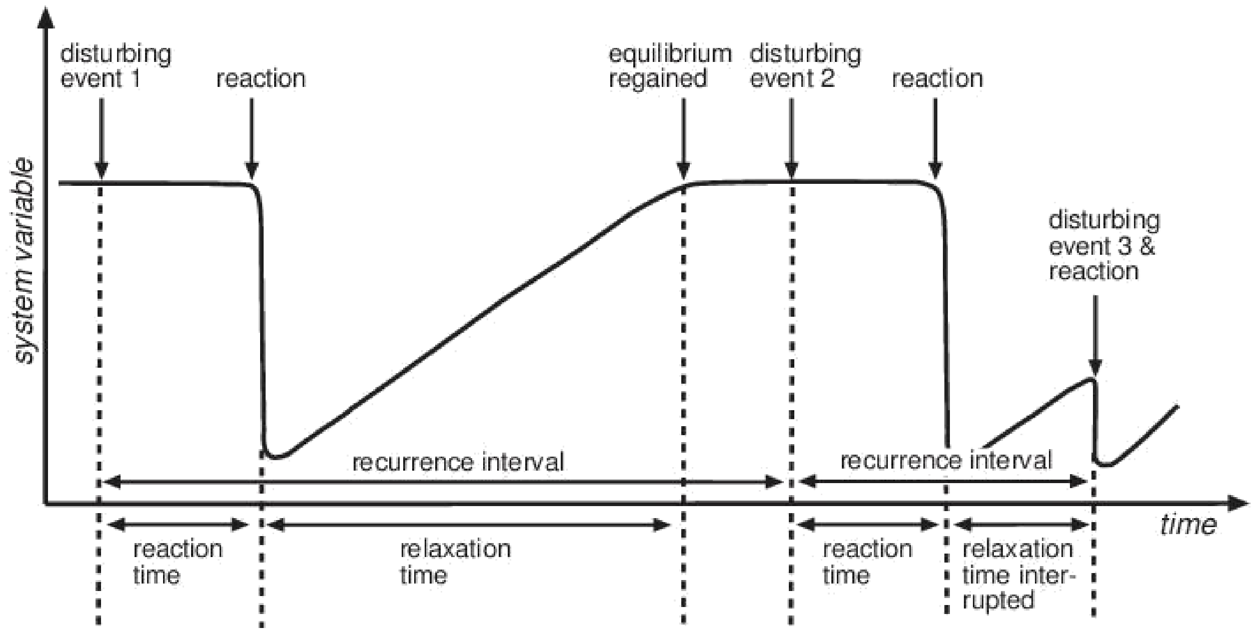

Figure 1.2: A schematic diagram visualizing the rate law within geomorphic systems (Hufschmidt et al., 2005). The diagram above shows both situations of reaching an equilibrium before a new disturbance event happens and a disturbance event occurring during relaxation time.

1.6 References

Tomkin, J. H., 2007, Coupling glacial erosion and tectonics at active orogens: A numerical modeling study: Journal of Geophysical Research, v. 112, F02015, doi:10.1029/2005JF000332

MacGregor, K.R., Anderson, R.S. and Waddington, E.D., 2009, Numerical modeling of glacial erosion and headwall processes in alpine valleys: Geomorphology, v. 103, no. 2, p.189-204.

Aitken, M.J., 1998, An Introduction to Optical Dating: Oxford University Press, 276 p.

Anderson, S.P., Anderson, R.S., Tucker, G.E., 2012a, Landscape scale linkages in critical zone evolution: Comptes Rendus Geoscience, v. 344, no. 11-12, p.586-596, doi:10.1016/j.crte.2012.10.008.

Benford, B., Crowley, J., Schmitz, M., Northrup, C.J., Tikoff, B., 2010, Mesozoic magmatism and deformation in the northern Owyhee Mountains, Idaho: Implications for along-zone variations for the western Idaho shear zone: Lithosphere, v. 2, p.93-118, doi:10.1130/L76.1.

Beranek, L.P., Link, P.K., Fanning C.M., 2006, Miocene to Holocene landscape evolution of the western Snake River Plain region, Idaho: using the SHRIMP detrital zircon provenance record to track eastward migration of the Yellowstone hotspot: Geological Society of America Bulletin, v. 118, p. 1027-1050

Berlin, M.M., Anderson, R.S., 2007, Modeling of knickpoint retreat on the Roan Plateau, western Colorado: Journal of Geophysical Research, v. 112, F03S06

Berndt, C., Yıldırım, C., Çiner, A., Strecker, M., Ertunç, G., Sarikaya, M.A., Özcan, O., Kıyak, N. G., & Öztürk, T., 2018, Quaternary uplift of the northern margin of the Central Anatolian Plateau: New OSL dates of fluvial and delta-terrace deposits of the Kızılırmak River, Black Sea coast, Turkey: Quaternary Science Reviews, v. 201, p. 446-469

Bestland, E.A., 1997, Alluvial terraces and paleosols as indicators of early Oligocene climate change (John Day Formation, Oregon): Journal of Sedimentary Research, v. 67, p. 840–855

Bonnichsen, B., Godchaux, M.M., 2006, Geologic Map of the Murphy 30 x 60 Quadrangle, Ada, Canyon, Elmore, and Owyhee Counties, Idaho: Idaho Geologic Survey Digital Web Map, no 80, scale 1:100,000

Bonnichsen, B., McCurry, M., Godchaux, M.M., 2004, Miocene Snake River Plain rhyolites of the Owyhee Front, Owyhee County, Idaho, Geological field trips in southern Idaho, eastern Oregon, and northern Nevada: U.S. Geological Survey Open-File Report 2004-1222, p. 154-173

Bracken L.J., Wainwright, J., 2006, Geomorphological equilibrium: myth and metaphor?: Transactions of the Institute of British Geographers, v. 31, p. 167– 178

Briant, R.M., Bates, M.R., Marshall, G.D., Schwenninger, J.-L., Wenban-Smith., F.F., 2012, Terrace reconstruction and long profile projection: a case study from the Solent River system near Southampton, England: Proceedings of the Geologists' Association, v. 123, p. 438-449

Brocard, G., Willenbring, J.K., Scatena, F.N., Johnson, A.H., 2015, Effects of a tectonically- triggered wave of incision on Riverine Exports and Soil Mineralogy in the Luquillo Mountains of Puerto Rico: Applied Geochemistry, v. 63, p. 586– 598

Brunsden, D., and Thornes, J.B., 1979, Landscape sensitivity and change: Transactions of the Institute of British Geographers, v. 4, p. 463–484

Bull, W. B., 1991, Geomorphic responses to climatic change: New York, Oxford University Press, 326 p.

Camp, V.E., Ross, M.E., Duncan, R.A., Jarboe, N.A., Coe, R.S., Hanan, B.B., Johnson, J.A., 2013, The Steens basalt: Earliest lavas of the Columbia River basalt group, in Reidel, S.P. et al., eds., The Columbia River flood basalt province: Geological Society of America, Special Paper 497, p. 87–116

Chase, A.S.Z., Weishampel, J.F., 2016, Using LiDAR and GIS to investigate water and soil management in the agricultural terracing at Caracol, Belize: Advances in Archaeology Practices, v. 4, p.357-370

Cook, K.L., Turowski, J.M., Hovius, N., 2013, A demonstration of the importance of bedload transport for fluvial bedrock erosion and knickpoint propagation: Earth Surface Processes and Landforms, v. 38, p. 683– 695, doi: 10.1002/esp.3313

Crosby, B.T., and Whipple, K.X., 2006, Knickpoint initiation and distribution within fluvial networks: 236 waterfalls in the Waipaoa River, North Island, New Zealand: Geomorphology, v. 82, p. 16–38, doi: 10.1016/j.geomorph.2005.08.023

DiBiase, R.A., Whipple, K.X., Lamb, M.P., and Heimsath, A.M., 2014, The role of waterfalls and knickzones in controlling the style and pace of landscape adjustment in the western San Gabriel Mountains, California: Bulletin of the Geological Society of America, v. 127, p. 539–559, doi: 10.1130/B31113.1

Ekren, E.B., McIntyre, D.H., Bennett, E.H., Malde, H.E., 1981, Geologic map of Owyhee County, Idaho, west of longitude 116 degrees W: USGS Numbered Series, no. 1256, scale:1:25,000, 2 sheets

Evans, J.S., Hudak, A.T., Faux, R. and Smith, A., 2009, Discrete return lidar in natural resources: Recommendations for project planning, data processing, and deliverables: Remote Sensing, v. 1, p. 776-794

Finnegan N.J. Balco G., 2013, Sediment supply, base level, braiding, and bedrock river terrace formation: Arroyo Seco, California, USA: Geological Society of America Bulletin, v. 125, p. 1114–1124, doi:10.1130/b30727.1.

Finnegan, N.J., 2013, Interpretation and downstream correlation of bedrock river terrace treads created from propagating knickpoints: Journal of Geophysical Research, v. 118, p. 54– 64

Finnegan, N. J., and W. E. Dietrich, 2011, Episodic bedrock strath terrace formation due to meander migration and cutoff: Geology, v. 39, 143–146

Flerchinger, G.N., Fellows, A.W., Seyfried, M.S., Clark, P.E., and Lohse, K.A., 2019, Water and carbon fluxes along an elevational gradient in a sagebrush ecosystem: Ecosystems, p. 1–18, https://doi.org/10.1007/s10021-019-00400-x

Gallen, S.F., Wegmann, K.W., Frankel, K.L., Hughes, S., Lewis, R.Q., Lyons, N., Paris, P., Ross, K., Bauer, J.B., and Witt, A.C., 2011, Hillslope response to knickpoint migration in the Southern Appalachians: Implications for the evolution of post-orogenic landscapes: Earth Surface Processes and Landforms, v. 36, no. 9, p. 1254–1267, doi: 10.1002/esp.2150.

Geach, M.R., Thomsen, K.J., Buylaert, J.P., Murray, A.S., Mather, A.E., Telfer, M.W., Stokes M., 2015, Single-grain and multi-grain OSL dating of river terrace sediments in the Tabernas Basin, SE Spain: Quaternary Geochronology, v. 30, p. 213-218

Gilbert, G.K., 1877, Report on the Geology of the Henry Mountains, U. S. Geog. Geol. Survey Rocky Mountain Region, 160 p.

Gomi, T., Sidle, R.C., Richardson, J.S., 2002, Understanding processes and downstream linkages of headwater systems: BioScience, v. 52, p. 905-916

Hancock, G.S., and Anderson, R.S., 2002, Numerical modeling of fluvial strath-terrace formation in response to oscillating climate: Geological Society of America Bulletin, v. 114, p. 1131-1142

Haneberg, W.C., 2005, The ins and outs of airborne LiDAR: an introduction for practicing engineering geologist: AEG News, v. 48, p. 16–19

Harkins, N., Kirby, E., Heimsath, A., Robinson, R., Reiser, U., 2007, Transient fluvial incision in the headwaters of the Yellow River, northeastern Tibet, China: Journal of Geophysical Research, v. 112, F03S04

Harley, S., and N., Kelly, 2007, Zircon: Tiny but Timely: Elements, v. 3, p. 13–18

Hufschmidt, G., Crozier, M., Glade, T., 2005, Evolution of natural risk: research framework and perspectives: Natural Hazards Earth System Science, v. 5, p. 375–387

Hughes, P.D., 2010, Geomorphology and Quaternary stratigraphy: the roles of morpho-, litho-, and allostratigraphy: Geomorphology, v. 123, p. 189-199

Karlstrom, L., Richardson, P. W., O'Hara, D., Ebmeier, S. K., 2018. Magmatic landscape construction: Journal of Geophysical Research: Earth Surface, v. 123, p. 1710–1730

King, L. C., 1953, Canons of landscape evolution, Geological Society of American Bulletin, v. 64, p. 721– 752

Lague, D., 2013, The stream power river incision model: Evidence, theory and beyond: Earth Surface Processes Landforms, p. 110 doi:10.1002/esp.3462

Lee, J., Williams, I., Ellis, D., 1997, Pb, U. and Th diffusion in nature zircon: Nature, 1997, v. 390, p. 159–162

Lian, O.B., 2013, Luminescence dating: optical dating: Encyclopedia of Quaternary Science, p. 653-66

Lindgren, W., and Drake, N.F., 1904, Description of the Silver City Quadrangle: U.S. Geological Survey Atlas, v. 104, p. 1-4

Litchfield, N.J., Berryman, K.R., 2005, Correlation of fluvial terraces within the Hikurangi Margin, New Zealand: implications for climate and base-level controls: Geomorphology, v. 68, p. 291– 313

Liu, X.Y., 2008, Airborne LiDAR for DEM generation: Some critical issues: Progressive Physical Geography, v. 32, p. 31–49

Lohse, K.A., Seyfried, M.S., Pierson., F.B., 2015, Managing the critical zone to obtain and sustain multiple benefits from working landscapes: The value of partnerships between LTAR and NSF CZO networks: American Geophysical Union, Fall 2015, Abstracts

McIntyre, D.H., 1972, Cenozoic geology of the Reynolds Creek Experimental Watershed, Owyhee County, Idaho: Idaho Bureau of Mines and Geology, pamphlet 151, 115 p.

Merritts, D.J., Vincent, K.R., Wohl, E.E., 1994, Long river profiles, tectonism, and eustasy: a guide to interpreting fluvial terraces.: Journal of Geophysical Research, v. 99, p. 14031– 14050

Moyle, P.R., Wallis, J.C., Bliss, J.D., Bolm, K.S., 2004, Digital Database of Selected Aggregate and Related Resources in Ada, Boise, Canyon, Elmore, Gem, and Owyhee Counties, Southwestern Idaho: U.S. Geological Survey Open-File Report 2004-1067, 560 p.

Mudd, S. M., 2016, Detection of transience in eroding landscapes: Earth Surface Process Landform, v. 42, p. 24–41, https://doi.org/10.1002/esp.3923

Murray, A.S., and Wintle, A.G., 2000, Luminescence dating of quartz using an improved single-aliquot regenerative-dose protocol: Radiation Measurements, v. 32, p. 57-73

Nasdala, L., Lengauer, C.L., Hanchar, J.M., Kronz, A., Wirth, R., Blanc, P., Kennedy, A.K., Seydoux-Guillaume, A.M., 2002, Annealing radiation damage and the recovery of cathodoluminescence: Chemical Geology, v. 191, p. 121–140

Norman, M.D., McElwee, K.R., Duncan, R.A., and Leeman, W.P., 1986, K-Ar ages of Oligocene Salmon Creek volcanics. Owyhee Mountains, Idaho: Isochron/West, v. 46, p. 9-14

Olszak, J., Kukulak, J., Alexanderson, H., 2016, Revision of river terrace geochronology in the Orawa-Nowy Targ Depression, south Poland: insights from OSL dating: Proceedings of the Geologists' Association, v. 127, p. 595-605

Pazzaglia, F.J., 2013, Fluvial terraces: In John, F.S., Treatise on Geomorphology: Academic Press: San Diego, p. 379– 412

Rasmussen, B., Fletcher, I.R., 2010, Dating sedimentary rocks using in situ U-Pb geochronology of syneruptive zircon in ash-fall tuffs <1mm thick: Geology, v. 38, p. 299–302, doi:10.1130/G30567.1.

Rhodes, E.J., 2011, Optically stimulated luminescence dating of sediments over the past 200,000 years: Annual Review of Earth and Planetary Sciences, v. 39, p. 461– 488

Robins, J. S., Kelly, L.L., Hamon, W.R., 1965, Reynolds Creek in southwest Idaho: An outdoor hydrologic laboratory: Water Resource Research, v. 1, p. 407– 413, doi:10.1029/WR001i003p00407

Rocha-Campos, A.C., Basei, M., Nutman, A., Kleiman, L., Varela, R., Llambia, E., Canile, F., and Darosa, C.R., 2011, 30 million years of Permian volcanism recorded in the Choiyoi igneous province (W Argentina) and their source for younger ash fall deposits in the Paraná Basin: SHRIMP U–Pb zircon geochronology evidence: Gondwana Research, no. 19, p. 509–523. doi:10.1016/j.gr.2010.07.003

Romer, R.L., 2003, Alpha-recoil in U-Pb geochronology: Effective sample size matters: Contributions to Mineralogy and Petrology, v. 145, p. 481– 491

Rubatto, D., 2002, Zircon trace element geochemistry: partitioning with garnet and the link between U-Pb ages and metamorphism.: Chemical Geology, v. 184, p. 123–138

Schanz, S. A., Montgomery, D. R., and Collins, B. D., 2019, Anthropogenic strath terrace formation caused by reduced sediment retention: Proceedings of the National Academy of Sciences of the United States of America, v. 116, p. 8734–8739

Schanz, S. A., Montgomery, D. R., Collins, B. D., and Duvall, A. R., 2018, Multiple paths to straths: A review and reassessment of terrace genesis: Geomorphology, v. 312, p. 12– 23.

Schoene, B., 2014, U-Th-Pb geochronology. In: Holland H.D. and Turekian K.K. (eds), Treatise on Geochemistry (second edition), Elsevier (Oxford), p. 341– 378

Seyfried, M., Lohse, K., Marks, D., Flerchinger, G., Pierson, F., and Holbrook, W.S., 2018, Reynolds Creek Experimental Watershed and Critical Zone Observatory: Vadose Zone Journal, v. 17, p. 1-20

Thouret, J.-C., 1999, Volcanic geomorphology—an overview: Earth-Science Review, v. 47, p. 95-131

Tofelde, S., Savi, S., Wickert, A.D., Bufe, A., and Schildgen, T.F., 2019, Alluvial channel response to environmental perturbations: Fill-terrace formation and sediment-signal disruption: Earth Surface Dynamics, v. 7, p. 609–631

Viveen, W., Schoorl, W.M., Veldkamp, A., Van Balen, R.T., Desprat, S., Vidal-Romani, J.R., 2013, Reconstructing the interacting effects of base level, climate, and tectonic uplift in the lower Mino River terrace record: a gradient modeling evaluation: Geomorphology, v. 186, p. 96-118

Wang, Y., 2005, The onset of the Tan-Lu fault movement in eastern China: constraints from zircon (SHRIMP) and 40Ar/39Ar dating: Terra Nova, v. 18, p, 423-431

Whipple, K.X., and Tucker, G.E., 1999, Dynamics of the stream-power river incision model: Implications for height limits of mountain ranges, landscape response timescales, and research needs: Journal of Geophysical Research: Solid Earth, v. 104, p. 17661–17674, doi: 10.1029/1999JB900120.

Whittaker, A.C., Boulton, S.J., 2012, Tectonic and climatic controls on knickpoint retreat rates and landscape response times: Journal of Geophysical Research, v. 117, p. F02024

Wintle, A. G., and Murray, A. S., 2006, A review of quartz optically stimulated luminescence characteristics and their relevance in single-aliquot regeneration dating protocols: Radiation Measurements, v. 41, p. 369– 391

Wohl, E., Brierley, G., Cadol, D., Coulthard, T.J., Covino, T., Fryirs, K.A., Grant, G., Hilton, R.G., Lane, S.N., Magilligan, F.J., Meitzen, K.M., Passalacqua, P., Poeppl, R.E., Rathburn, S.L., Sklar, L.S., 2019, Connectivity as an Emergent Property of Geomorphic Systems: Earth Surface Processes Landforms, v. 44, p. 4-26

Wood, S.H., Clemens, D.M., 2002, Geologic and tectonic history of the western Snake River Plain, Idaho and Oregon, Tectonic and Magmatic Evolution of the Snake River Plain Volcanic Province: Idaho Geological Survey Bulletin, v. 30, p. 69–103

Yan, Q., Iwasaki, T., Stumpf, A., Belmont, P., Parker, G., Kumar, P., 2018, Hydrogeomorphological differentiation between floodplains and terraces: Earth Surface Process Landforms, v. 43, p. 218–228

Chapter 2. The Topographic Evolution and Surficial Geology of Reynolds Creek

2.1 Introduction

2.1.1 Problem Statement

RC can be defined as a sedimentary fill basin that follows basic fill and cut sequences. The fill of this sequence is the key attribute into understanding how the fill and cut sequences unraveled, and is the tool to be see back into past events. Presence of this fill, known as the Sedimentary fill of Reynolds Creek, throughout the basin can establish a better framework for when (using U-Th-Pb geochronology) and how (using surficial landform mapping and topographic analysis) the filling of the basin influenced the topography. This knowledge can be used to better understand the mechanisms for how landslide and volcanically dammed basins fill and maintain its basin deposits.

2.2 Setting

2.2.1 Regional Setting

RC is a 238 km^2 drainage basin that flows into the Snake River in southwestern Idaho. RC is located 40 miles south of Boise and 14 miles east of the Oregon-Idaho border. The drainage basin is located within six USGS quadrangles: Soldiers Cap, Rooster Comb Peak, De Lamar, Silver City, Reynolds, and Wilson Peak. Topographically, RC has a large spread of elevations, ranging between 1000 and 2250 meters above sea level (Figure 2.1). There is a large change in elevation between basin floor in the north, which ranges 1050 to 1350 meters above sea level, and the surrounding highlands, which range between 1350 to 2250 meters above sea level. Smaller tributaries in RC are larger focuses for research within the CZO, such as intermittency in streams within Murphy

Creek, sediment suspension and discharge within Salmon Creek, and rain to snow transition within Johnston Draw (Pierson et al., 2000; Godsey et al., 2018; Warix et al., 2020). RC has a mean annual maximum temperature of 15.6°C and a mean annual minimum temperature of 0.7°C (Hanson et al., 2001). The drainage basin is a semi-arid basin, with a mean annual precipitation of 462 millimeters and a mean annual snow-water contribution of 191 millimeters (Seyfried et al., 2018).

2.2.2 Geologic History

The RC was established as a Critical Zone Observatory in 2014 with a focus on quantifying soil carbon and the processes that control its development and mobility within the watershed. Numerous geologic studies occurred in the area (Lindgren and Drake, 1904; McIntyre, 1972; Ekren et al., 1981; Bonnichsen and Godchaux, 2006). My map largely builds on the highest resolution geology mapped by McIntyre (1972).

McIntyre (1972) mapped RC, and the map has only been updated to largely add ages to the geologic units (Figure 2.2) (Bonnichsen and Godchaux, 2006). The basement rocks consist of Cretaceous granitoid intrusions that are from the Idaho Batholith and are deformed in the southernmost extent of the Idaho shear zone and the Idaho Batholith (Beranek et al., 2006; Benford et al., 2010). This intrusive suite, called the Silver City granite, was exhumed at the onset of a long period of Miocene extrusive igneous events. The Salmon Creek porphyritic olivine basalts have a whole rock K-Ar age between 30.9 and 26 Ma, and were deposited on top of the Silver City granite (Norman et al., 1986). Steens Mtn. Basalts with an Ar-Ar age of 16.73±0.16 Ma, were next extruded from local dikes over the Salmon Creek basalts and the Silver City granite (Camp et al., 2013).

Reynolds Creek basin (Figure 2.2) is interpreted to have been created and filled with volcaniclastic sediment after the deposition of the Steens Basalts (McIntyre, 1972). These deposits include silicic tuffs, diatomites, lignites, ash and other fine lacustrine sediments. The deposits and the normal faults present throughout the northwestern part of Reynolds Creek define the Reynolds Creek basin to be a closed depression within an extensional graben. The Reynolds Creek basin sediments were deposited contemporaneously with various volcanic rocks during regional crustal extension in the mid-Miocene (McIntyre, 1972). These volcanic rocks include latites, ash-tuffs, and rhyolites. The Reynolds Creek rhyolite erupted at the northern end of the basin at 11.48±0.09 Ma, shortly after the western Snake River Plain graben fill (Figure 2.2) began to subside and bedrock and overlapping the Reynolds Creek basin sediments (Bonnichsen et al., 2004). The Rhyolitic lava flow of Reynolds Creek down a north-draining paleocanyon of Reynolds Creek until reaching the standing water. Drainage was re-established after 11.48 Ma toward the Snake River Plain, which incised the Reynolds Creek rhyolite and the Silver City granite to create the outlet stream present today.

<u>2.3 Methodology</u>

2.3.1 Map Making

The surficial geologic map of RC was created by processing DEM data that was obtained for BSU by the NASA Terrestrial Ecology NNX14AD81G. The DEMs were processed using the *hillshade* and the *slope* tool to create base maps used to create polygons. Polygons were mapped using both photos and LiDAR. These polygons were initially mapped at a 1:35000 scale, and were refined to 1:10000 scale in accuracy.

Over the summer of 2020, I ground-truthed the mapped polygons. I modified the polygon shapes using tablets with GPS capabilities. Alongside landform mapping, I obtained descriptions of map units and performed additional analysis, such as measuring sections for the stratigraphic columns and surveying locations for geochronologic analysis. I updated the polygon maps every two weeks. I also created a mapping effort to follow and measure the maximum elevation of the Sedimentary Fill of Reynolds Basin group throughout the basin and record location and elevation.

Sections were measured for the Sedimentary Fill of Reynolds Creek for both context of geochronology results and to describe the sedimentology. Each measured section was accurate to the decimeter scale, with dips updated throughout the section. The dip at all measured intervals remained relatively consistent (between two to three degrees). The strike and dip of each of the sections were consistently striking north and shallowly dipping (~350/15). These measured sections were then drafted into three stratigraphic columns (reference strat columns). Correlation between all the stratigraphic columns is unknown as there is no clear marker bed that is consistent between the three stratigraphic columns. Each of the stratigraphic columns were drafted by hand and then digitized in Adobe Illustrator.

2.3.2 Geochronology

2.3.2.1 U-Th-Pb

Four samples of the Sedimentary Fill of Reynolds Creek were collected from three distinct outcrops. These locations have been named the Pinnacle, the Summit, and the Quarry (Figure 2.1). Each sample was marked with GPS locations, markers in the ground to find locations on future visits, and plotted in ArcGIS Collector in order to obtain elevation of the site. ~Five pounds of sample were collected for each sample. These samples were transported to the

Isotope Geology Lab (IGL) at Boise State University in Boise, Idaho where all analysis will take place.

Sample preparation involved zircon grains being separated from the collected samples. These zircon grains were separated from samples using conventional crushing, grinding and water table techniques, followed by heavy liquid and mineral separation using the IGS mineral separation guide. These zircon grains underwent additional prep of minor annealing in a furnace, mounted in epoxy, and imaged with CL imagery. These images allowed for sites to be selected for LA-ICPMS on the zircon. Sites chosen were based on the overall integrity of the grain (no cracks or extensive damage) and zonation placement (sites were not selected if on the boundary of a zonation).

Samples underwent LA-ICPMS to determine if the grains were primary or detrital in origin. This determination was deduced through looking at the peaks present within an LA-ICP-MS spectrum. If multiple age peaks were present within the sample, then the sample was determined as detrital, while if one age peak was present within the sample, it was determined as primary. This determination was required as samples undergoing CA-ID-TIMS would not represent the formation timing of the grains. 45 zircon grains were selected to undergo CA-ID-TIMS analysis based on the set criteria.

Sample preparation for CA-ID-TIMS were based on the IGL sample preparation guide. Samples were dissolved and underwent the chemical procedures to be placed within the mass spectrometer. Samples underwent CA-ID-TIMS analysis to give more precise dates for the grains collected.

All data were processed and exported into a template excel sheet that allows for the data to be calculated. The excel sheet determined the date of these samples. Processed data for LA-ICP-MS data was plotted into Population Density Function using ISOPLOT, while processed data from CA-ID-TIMS was plotted on a Concordia (Appendix 1).

2.3.2.2 OSL

Three OSL samples were collected from three locations (Figure 2.1). These samples were collected following the protocol provided by Utah State University. Using the metal tube approach, sand lenses were defined through analysis of outcrops. These sand lenses were only considered if the depth below the surface was greater than one meter. Foam was cut and fitted onto the end of the tube, then capped to prevent light exposure as the tube was hammered into the sand lense. Once hammered in, two ancillary samples sampling materials were collected; a moisture content sample that is obtained from grabbing sediment that surrounds the features and placing them inside a film cannister, and half full quart bag of the environmental dose rate that was used for calibration. The dose rate sample is collected through digging around the 30 cm diameter of the experimental sample. Once the two ancillary samples are collected, the tube is gently removed from the outcrop and the end is packed tightly with sediment to prevent any mixing. The sample is then capped off, and taped tightly.

Samples are processed at the Utah State University Luminescence lab, and undergo a single-aliquot regenerative-dose procedure for OSL dating of quartz sands (Wintle and Murray, 2006). This procedure begins with the measuring of the natural luminescence from the experimental sample to determine the dose equivalent. The bleached experimental samples are then given known radiation doses to create a luminescence dose-response curve. The dose equivalent is then obtained through the calculating the intercept of the natural luminescence signal on the luminescence dose-response curve (Appendix 3). The environmental dose rate sample had its dose rate calculated. As a consequence of COVID-19 restrictions, samples were sent to the USU lab for analysis instead of personally being able to process and analyze the samples

2.3.3 Topographic Analysis

To establish the longitudinal profile of the basin, the DEM of RC was loaded into MATLAB and underwent analysis using the Topographic Analysis Kit (TAK) along with TopoToolbox (Schwanghart and Scherler, 2014; Forte and Whipple, 2018). The DEM of RC was processed using the *MakeStreams* tool, the *FindThreshold* tool, the *SegmentPicker* tool, and the *SegmentPlotter* tool to visualize and extract the stream profile from Reynolds Creek stream. The latitude, longitude, elevation, and distance from mouth were extracted from MATLAB into a .txt file.

The .txt file was loaded in and georeferenced within the DEM map of RC in ARCGIS Pro. This allowed for the .txt file data to be visualized on the map. This data is then used for an empirical kriging with a Bayesian modelling approach to create a DEM for a straight line stream to be based on. A straight stream is generated to prevent errors in elevation. Each of these points are spaced every 30 meters from the mouth of the stream, along with extracting the elevation from the kriged DEM surface (e.g. Wehrs, 2018). Terrace elevation points are placed along the center then extracted from the Reynolds DEM. These terrace points are spatially joined with the stream elevation points, joining the elevation of the terraces and their ID to the latitude, longitude, and distance from mouth of stream from the .txt file of the Reynolds Creek stream. This data is exported from ARCGIS Pro into excel, where the headings were modified so loading into MATLAB would be streamlined.

` Both the terrace elevation profile and the Reynolds Creek stream profile were plotted on one longitudinal profile. A script was written in MATLAB to iteratively plot the terrace data (Appendix 1).

<u>2.4 Results</u>

We organize the presentation of the results by timing of the map units. Each section will briefly go over the morphology of the sediments, the locals the unit is present at, and other information obtained from those sediments.

2.4.1 Overview

A 1:50000 scale surficial geologic map was created and is interpreted further below (Attached Map and Figure 2.3). The general overview of the map is focused in two parts; the lower basin that has presence of the Sedimentary Fill of Reynolds Creek, and the upper basin that does not have the presence of the Sedimentary Fill of Reynolds Creek. The separation of the two sections helps further define the processes that are present within the basin, and show the separation of hillslope and channel processes occurring within the landscape.

A correlation of map units (CoMU) was created and is based on crosscutting relationships and geochronology where relevant. The CoMU is used as an organizational guide for the evolution of RC. A large scale publishable version of the map (Plate 1), along with a shortened description of the mappable units, will be submitted to the Idaho Geological Survey.

Soil types and loess mantling are not addressed in this study. This information is not pertinent to the overall evolution of RC. Future work may incorporate this material onto the map.

2.4.2 Bedrock

<u>2.4.2.1 Granitic Bedrock</u>

The granitic basement is a coarse-grained quartz monzonite of variable color present throughout Reynolds Creek. The granitic basement is largely represented in the upper basin and is Cretaceous in age (Benford et al., 2010). The granitic basement rock contains quartz, orthoclase, biotite, muscovite, and small amounts of plagioclase. The granite occurs as rounded domes with visible granular decomposition textures.

The granitic bedrock resides in topographically high places within the basin and is largely concentrated on the western side of the basin. Granitic bedrock outcrops are seen between 1825 to 1622 meters above sea level. The pockets of outcrops are largely associated with the delineation of the Reynolds Creek watershed on this side of the basin. Outcrops of the granitic bedrock can also be seen on the eastern side of the upper basin towards the edge of the map area as well, and are 1975 to 2250 meters above sea level. The granitic bedrock outcrops on the eastern side of the basin are significantly smaller when compared to outcrops on the western side of the basin.

2.4.2.2 Volcanic Bedrock

The volcanic bedrock is a widespread volcanic unit that encompasses 75% of the underlying bedrock within the basin. The majority of this volcanic bedrock is consistent of olivine rich basalts, particularly present on the eastern side of the basin. Other volcanic rock units include latites, tuffs, rhyolites, and andesites. Volcanic bedrock deposition occurs within pulses, starting at the Salmon Creek porphyritic olivine basalts which have a whole rock K-Ar age between 30.9-26 Ma to the final pulse of the Rhyolitic lava flow of Reynolds Creek with an Ar-Ar age of 11.48 Ma (Norman et al., 1986; Bonnichsen et al., 2004). The activity of these pulses are associated with the Yellowstone Hotspot track, the subsidence and formation of the western Snake River Plain and Idaho-Oregon Graben respectively (Wood and Clemens, 2002; Hooper et al., 2002).

Bedrock for the volcanic rock is largely dominated in the upper basin and sometimes exposed in stream channels within the lower part of the basin. For example, a felsic latite cuesta is located just to the east of the ARS quonset building (Figure 2.4) right on the border of the alluvial sediments. These large outcrops appear to only persist on the eastern side of the basin, and are north-south trending. Elevations for these outcrops average around 1366 meters above sea level.

Volcanic bedrock presence in RC is focused in areas of high topography and minimal relief, such as on top of most of large hills. Larger outcrops of the volcanic bedrock are present on the eastern side of the basin, whereas there are smaller but more plentiful outcrops of volcanic bedrock present on the western side of the basin. In particular, the Salmon Creek porphyritic olivine basalts contain large quantities of small outcrops on the northwestern part of the basin. Elevations for these outcrops are between 1500 to 2250 meters above sea level.

Evidence of faulting is present within the volcanic bedrock. Normal faults are found with the down thrown side to the Northeast. This allows for major tilting to occur within the volcanic bedrock.

2.4.3 Colluvium

Colluvium is defined as loose unconsolidated material that is deposited at the bottom of slopes. Mechanism for colluvium deposition include sheetwash and mass wasting processes, and appear in various grain sizes.

2.4.3.1 Granitic Colluvium

Granitic colluvium is a pinkish-white angular boulder to pebble sized deposit found on hillslopes adjacent to or overlying granite bedrock hillslopes. Thickness of the granitic colluvium is variable depending on locations, with some as thick as five meters to as thin as 0.25 meters. This thickness is largely dependent on the relief and aspect of the slope for which the colluvium is mantling.

Presence of the granitic colluvium is often inconsistent, with discontinuities due to granite outcrops. At several locations, granitic colluvium was interfingering with volcanic colluvium. An estimated age on the granitic colluvium would be in the mid-Quaternary based soil development at observed locations.

2.4.3.2 Volcanic Colluvium

The volcanic colluvium is an angular boulder to pebble sized deposit on hillslopes within the upper basin. Thickness is variable and dependent on the aspect and relief of the slopes. Thickness is between 3 to 0.3 meters thick. The color of the volcanic colluvium is consistent with its source rock material. In general, colors are either seen to be reddish-grey on the eastern side of the basin and black toward the southern and western side of the basin.

Presence of volcanic colluvium is inconsistent, with discontinuities based on presence of outcrops, fluvial, or man-made deposits. These processes move or remove the colluvium present within these landscapes. At some localities, the volcanic colluvium overlies the granitic colluvium, while at localities the volcanic colluvium interfingers with the granitic colluvium. An estimated age of the volcanic colluvium of mid-Quaternary based on soil development at observed locations. Volcanic colluvium can be found throughout the upper basin. It is most prevalent along the eastern side of the upper basin, where the volcanic bedrock is more widespread and more dominated by volcanic processes. Most of the volcanic colluvium lies at elevations greater than 1350 meters above sea level. Presence decreases with elevation. Process for what caused the scarcity is unclear. Some landslides are present within the landscape, but would not explain the entirety of scarcity.

2.4.4 Sedimentary Fill of Reynolds Creek

2.4.4.1 Overview

The Sedimentary Fill of Reynolds Creek is an unconsolidated lacustrine deposit located largely on the western side of the lower basin. It is composed of diatomaceous bioclastic clay, ashfall tuff, inorganic fissile clastic clay, pumice, and lignite deposits. Presence of lignite and pumice is inconsistent. U-Th-Pb geochronology was performed on primary ashfall tuff beds within the unit to better constrain the timing of deposition.

The Sedimentary Fill of Reynolds Creek outcrops variably throughout the basin. On the western side, both distinct beds are found alongside pockets of the Sedimentary Fill of Reynolds Creek. These pockets are seen highest at 1350 meters and steadily decrease toward the southern extent. The Sedimentary Fill of Reynolds Creek does not appear on the eastern side of the basin except in small pockets near the present stream channel or toward the northeastern corner of the basin where a bedded section can be seen adjacent to volcanic bedrock. The thickest section is 105 meters, but is thought to extend under the surface.

2.4.4.2 Stratigraphic Elements

Stratigraphic columns were drafted for three localities of the Sedimentary Fill of Reynolds Creek: Pinnacle, Quarry, and Summit (Figure 2.1). These columns were created to (1) attempt to correlate columns with the use of geochronology to better understand the locatities, (2) capture the overall variability of the Sedimentary Fill of Reynolds Creek, and (3) document the sedimentological character of the unit. The columns represent the type section (Pinnacle), a slope face cut (Quarry), and one of the few locations present on the eastern side of the basin (Summit).

At the Pinnacle Location (Figure 2.5), the section alternates between diatomaceous clay, fissile clay, and ash dominated material. Clay is used to describe the grain size rather than the mineralogy of the unit. Small ash beds appear at the start, 9 meter mark, and the 45 meter mark, but the diatomaceous clay dominates the majority of the first 55 to 60 meters of the stratigraphic column. The first sample from the Pinnacle site was collected at 45 meter mark ash bed. A switch in the depositional material occurs at the 60 meter mark, which is started by an unconformity. Shortly above the unconformity, a paleosol is mapped within the stratigraphic column. Above the paleosol, the lacustrine clastic clay is fissile and likely sourced from upland sources and carried into the lake as a suspension. The fissile terrestrial clay has beds of ash between depositions, and the ash layers progressively getting larger toward the top of the column. A sample was collected at the third ash bed, labelled #3 and collected at the 70 meter mark (Figure 2.5). The largest ash bed present in any of the locations is at 83 meters, and extends just past 90 meters. This ash was massive and blocky, and was unfit for geochronology due to possible reworking.

At the Quarry Location (Figure 2.5), the clay present within the stratigraphic column is largely dominated by fissile terrestrial clay. Small ash and pumice beds are present at variable elevations within the stratigraphic column. These include at around four meters, which was the ash bed that the sample was collected. A pumice is found at just under ten meters, and a large blocky ash deposit begins around 24 meters. The fissile clay gets more platey heading up section.

At the Summit Location (Figure 2.5), the stratigraphic column shows interactions between the Arkosic Unit and the Sedimentary Fill of Reynolds Creek. The Arkosic Unit (discussed in a later section in detail) underlies the area by about 15 meters. The Arkosic Unit is worked into the first outcrop of the ash fall tuff, where the sample from the geochronology was obtained. This ash continues with a small break from a covered section until just under the 30 meter mark, where a small bed of diatomaceous clay appears. This bed progresses about 5 meters, and is topped by more ash.

2.4.4.3 Geochronology

All data in the first paragraph is from LA-ICP-MS analysis, while all data from the second paragraph are from CA-ID-TIMS analysis.

For the Pinnacle locality, samples #1 and #3 were collected and ran. the probability density at sample location #1 shows a large peak in the middle to late Miocene with some small inheritance from the Late Cretaceous (Appendix 2 and Table 2.1). The mean date that was calculated is 10.70±0.18 Ma with 0 of the 57 grains plotted rejected. This data shows an error margin of around 1.7%. The probability density at sample location #3 shows a large peak in the middle to late Miocene with a small peak present in the mid Eocene (Appendix 2 and Table 2.1). The mean date that was calculated is 10.62±0.23 Ma with 0 of the 57 grains plotted rejected. This data shows an error of margin around 2.3%. A distribution was made for sample #1 at the Quarry locality. The probability density at this location shows a large peak in the middle to late Miocene with some small inheritance from the Late Cretaceous (Appendix 2 and Table 2.1). The mean date that was calculated is 10.69±0.36 Ma with 0 of 31 grains rejected. This data shows an error margin of 3.3%. A distribution was also made for sample#1 at the Summit locality. The probability density at this location shows a large peak in the middle to late Miocene along with a large peak present in the Late Cretaceous (Appendix 2 and Table 2.1). The mean date that was calculated is 10.98±0.36 Ma with 0 of 24 grains being rejected. This date was determined based of the distribution of the lower peak, excluding the data that was inherited in the Late Cretaceous. This data shows an error margin of 3.3%.

For both sites at the Pinnacle location, eight total zircons underwent analysis. For sample #1 at the Pinnacle locality, we calculated a weighted mean $^{206}Pb/^{238}U$ date of 10.986 ± 0.009 Ma, with a mean squared weighted density (MSWD) of 0.98. For sample #3 at the Pinnacle locality, we calculated a weighted mean $^{206}Pb/^{238}U$ date of 10.366 ± 0.009 Ma, with a MSWD of 0.90. For samples located at the Quarry and Summit locatities, seven total zircons underwent analysis. For the sample at the Quarry, we calculated a weighted mean $^{206}Pb/^{238}U$ date of 10.989 ± 0.027 Ma, with a MSWD of 0.32. For the sample at Summit, we calculated a weighted mean $^{206}Pb/^{238}U$ date of 11.127 ± 0.008 Ma, with a MSWD of 1.12. An additional sample was collected from the Rhyolitic lava flow of Reynolds Creek to be used for comparison. Nine zircons underwent analysis from the Rhyolitic lava flow of Reynolds Creek. For the sample from the Rhyolitic lava flow of Reynolds Creek, we calculated a weighted mean $^{206}Pb/^{238}U$ date of 11.413 ± 0.006 Ma, with a MSWD of 0.67. Additional data is found in the appendix (Appendix 2).

2.4.5 Older Terraces (Qt_o)

The older terraces within RC are large, gravel-to-cobble-capped strath terraces that are 1350 meters above sea level located on the western side of the lower basin. White sediment representative of the Sedimentary Fill of Reynolds Creek is eroded to make the strath. The gravel cap for these terraces is composed of four different rock types: reddish-brown subrounded to rounded olivine basalts, ranging in size from boulders to very coarse sand, gray subrounded andesite/basalt, ranging from boulder to pebble, red rounded volcanic pumice, cobble sized, fairly low density, and boulder sized granite, large crystals of feldspar and quartz. Of these four cap rocks, the red olivine basalt is around 80 percent of the terrace cap. The older terrace's trend is ENE-WSW trend. No paleochannels are present around the channel, so flow direction cannot be determined. Date of the older terraces is unknown, but future OSL data may better constrain the timing of this event.

2.4.6 Mid Terraces (Qt_m)

The mid terraces within Reynolds Creek are large gravel capped terraces are 1270 to 1300 meters above sea level located on the western side of the lower basin. White sediment representative of the Sedimentary Fill of Reynolds Creek is the strath for the terrace. The gravel cap for these terraces is composed of four different rock types: red subrounded-to-rounded olivine basalt, ranging in size from boulders-to-coarse sand, gray subrounded andesite/basalt, ranging in size from boulder-to-pebble, red rounded volcanic pumice, cobble sized, fairly low density, and boulder sized granite with large crystals of feldspar and quartz. Though compositionally similar to the older terraces, the mid terraces cap is a finer grained andesite. The trends of the terraces are SSE-NNW, pointing toward the current outlet. No paleochannels exist in the region, which prevents a clear stream direction from being determined. Timing of the mid terraces are unknown, but are assumed to be Quaternary in age.

2.4.7 Younger Terraces (Qt_y)

The younger terraces within Reynolds Creek are gravel capped terraces that are 1250 to 1220 meters above sea level located on the eastern and western side of the lower basin. The terraces are alluvial fill terraces, with the alluvial fill composed of coarse grained granitic sands with rounded reddish gray boulder to pebbles. The gravel cap for these terraces is composed of four rock types: red subrounded to rounded olivine basalts, ranging in size from boulders to very coarse sands, gray subrounded andesite/basalt, ranging in size from boulders to pebbles, red rounded volcanic pumice, cobble sized, fairly low density, and boulder sized granite, large phaneritic crystals of feldspar and quartz. While the rock types are consistent with what is seen on the other non-contiguous terraces, terrace cap is more variable in composition based on location. Smaller sized granite cap is the cap on the eastern side of the basin, while smaller sized gray subrounded andesites are the western terrace's caps. The younger terrace's trend always points towards the current outlet of Reynolds Creek, giving trends of either ENE-WSW on the western side and WNW-ESE on the eastern side of the basin. No paleochannels are present around the channel, so flow direction cannot be determined. It is likely a Quaternary terrace.

2.4.8 Contiguous Terraces

2.4.8.1 Qt4

Qt4 represents the fourth lowest terrace. Qt4 is a strath terrace composed of volcanic material sourced from the eastern side of the basin. A small alluvial deposit is present, which is composed of volcanic cobbles. These cobbles are plentiful, with only smaller pockets of sand present within the slope face. Sand lenses are present in small variable amounts around three to three and a half meters below the surface, located in the lower section of the B_t layer. Cement for the grains is largely silicate in nature, with small lenses in the B_t layer that contains calcium carbonate cement on the rocks.

Qt4 is found in the southern and center part of the lower basin. Elevation wise, the maximum elevation of Qt4 is around 1280 meters above sea level, but is always around 12 to 17 meters above the current stream level. In terms of width, it is the most variable of the terraces, with the maximum width of around 780 meters and at minimum around 33 meters. One sample was collected for OSL at this terrace.

2.4.8.2 Qt3

Qt3 represents the third lowest terrace. Qt3 is a strath terraces cutting into underlying volcanic material on the eastern side of the basin. Within the terraces, a thin alluvial fill deposit is present that is composed of gravel sized grains of either granitic or volcanic origin. This particular terrace is capped by loess deposits. Sand lenses are present within the terrace, and are often located around 2 meters below the surface. Cementing on the grains are silicate dominated in most layers, but in the B_t1 and B_t2 layers, the cementing is calcium carbonate dominated.

Qt3 is entirely present within the center of the lower basin. Elevation wise, the maximum elevation Qt3 is seen at 1215 meters above sea level, but ranges between eight to twelve meters above the current stream elevation. In terms of the width of the terrace, it is significantly more consolidated and less variable than Qt4, with the maximum width being 300 meters and the minimum width being around 33 meters. Two samples were collected from this terrace for OSL.

2.4.8.3 Qt2

Qt2 represents the second lowest terrace. Qt2 is a strath terrace composed of volcanic material sourced from the eastern lower basin. Alluvial fill canvases the riser of the terrace, consisting of small cobble to pebble sized grains derived from granitic or volcanic sources. The dominant gravel type is mainly volcanic. The color of the sand cement turns yellowish green below the two meter mark. Sand lenses are present within the deposit, located around the two to two and a half meters below the surface. Loess does cap the terrace, only around a meter down from the top of the terrace. The sand is silica cemented.

Qt2 is dominantly in the center of the basin, with little variability in location. Qt2 is found at its highest around 1210 meters above sea level, but compared to the stream is only found at most 5 to 8 above the current stream elevation. Width of Qt2 at its widest 400 meters and at its thinnest around 80 meters.

2.4.8.4 Qt1

Qt1 is the lowest terrace within RC. Qt1 is both a strath terrace cutting into volcanic material sourced from the eastern side of the basin, and a fill terrace that accumulated the Sedimentary Fill of Reynolds Creek toward the western side of the basin. Charcoal deposits are present within the terrace in small twigs and fragments. Small deposits of alluvial fill material that is composed of cobbles to pebbles sourced from volcanic material are found in the terrace. Some areas of the cement are composed of calcium carbonate in the upper B_t layer, but is largely composed of silica.

Location of Qt1 is the most variable. It is the most widespread, present on all sections of the lower basin. Qt1 is present at highest around 1270 meters above sea level, but does not exceed more than two to three meters above where the current stream. Qt1 is also one of the few terraces to be present along some of the other major tributaries, especially present in the north where Qt1 is present along the Salmon Creek. Qt1 is variable in width as well, being the widest at around 500 meters and thinnest at around 35 meters.

2.4.8.5 Geochronology

Three OSL samples were obtained and processed. The locations (Figure 2.1) the samples were collected represent ages of the older contiguous terraces. One sample was collected from Qt4, and two samples were collected from Qt3: one from the overlying loess layer, and one from the sand lense of within a trench on the terrace.

For the sample collected from the sand lense from Qt3, the OSL age was found to be 30.02 ± 4.76 ka (Appendix 3 and Table 2.2). The sub fraction sample showed that this sample has a fine grained sand percentage at 60%, with a medium fraction of 20% and a coarse fraction of 20%. The in-situ water content was high at around 20.0%.

For the sample collected from the overlying loess on Qt3, the OSL age was found to be 22.30 ± 3.37 ka (Appendix 3 and Table 2.2). The sub fraction sample showed that this sample has a fine grained sand percentage at 85%, with a medium fraction of 5% and a coarse fraction of 10%. The in-situ water content was high at around 19.2%.

For the sample collected at Qt4, the OSL age was found to be 29.09 ± 4.25 ka (Appendix 3 and Table 2.2). The sub fraction sample showed that this sample has a fine grained sand percentage at 75%, with a medium fraction of 25% and a coarse fraction of 5%. The in-situ water content was low at around 2.8%. Further data is present in Appendix 3.

2.4.9 Alluvial Sediments

2.4.9.1 Overview

The alluvial sediments are composed of pebble to fine sand sized grains that were deposited on either terrace tops or on the alluvial floor. This sediment is defined by three sources: (1) coarser grained alluvial sediments derived from granitic bedrock, (2) finer grained alluvial sediments derived from granitic bedrock/colluvium, and (3) finer grained alluvial sediments derived from the volcanic bedrock/colluvium.

2.4.9.2 Arkosic Unit (Ta)

The Arkosic Unit is the coarser grained alluvial sediment derived from the granitic bedrock. The eastern side of the basin is present with this sediment. The origin for this sediment is unclear, as no intermixed volcanic grains are present within the sample. Compositionally, the Arkosic Unit is dominated by quartz, orthoclase, biotites, and some plagioclase. This composition differs from the granite bedrock in the lack of muscovites.

The Arkosic Unit is both unlithified and lithified. Lithified Arkosic Unit was at some localities disturbed by hydrothermal activity, based on the presence of opal veins found present within the sediment. The lithified Arkosic Unit is massive, blocky and mimics a similar appearance to the granitic boulders. Lithified Arkosic Unit is distinguishable from granitic boulders through presence of sedimentary structures, such as cross-bedding.

The Arkosic Unit is only located within the lower basin, and dominantly is present on the eastern side of the lower basin. The cross cutting of the Arkosic Unit is inconsistent and confusing when compared to previous literature. Localities observed on the northeastern side of Reynolds Creek show the Arkosic Unit underlying the Sedimentary Fill of Reynolds Creek, but on the western side of the basin, the Arkosic Unit overlies the Sedimentary Fill of Reynolds Creek. Elevation-wise, the Arkosic Unit is present below 1275 meters below sea level. Evidence of Arkosic Unit can be seen within the alluvial floor, but is distinguishable from the alluvial floor sediments due to its coarseness.

2.4.9.3 Alluvial Wash (Qta)

The alluvial wash are sediments are fine grained, well rounded sediments that are deposited in the flood plain of the modern streams. These sediments are largely composed of Colluvial and Bedrock material that is sourced from either a granitic or volcanic source. Color of these sediments are correlated with the source, but are dominantly reddish black.

The alluvial wash unit is closely related to the stream channel, and is overall broader in the lower basin than in the upper basin. There are pockets within the upper basin, particularly just preceding landslides, that sees the alluvial wash expand to a wider capacity (200 to 300 meters) than the average (50 to 75 meters). Presence of the alluvial wash is largely in the lower basin, and focused mainly on Reynolds Creek. Other locations have alluvial washes that are a greater size, such as near the mouth of Salmon Creek.

2.4.10 Landslides (Qls)

Landslides are present throughout large sections of the upper basin, though large portions of these landslides are heavily covered by vegetation. These landslides are largely composed of rotational slumps, with clear scarps present in the LiDAR of Reynolds Creek. Small localized topples are present in the lower basin toward the eastern and northern sides of the lower basin, but are in general too small to be mapped. These landslides are almost exclusively present within areas of volcanic bedrock.

Landslide deposits within Reynolds Creek are variable in elevation, but are consistently above 1400 meters in elevation. Landslide sizes are between 305 to 3000 meters long. Landslides are located mostly within the southern section of Reynolds Creek upper basin, and toward the northwestern side of the upper basin. This seems largely correlated with higher slope reliefs.

2.4.11 Longitudinal Stream Profile and Terraces

Two profiles reflect the current topography. A total longitudinal profile of Reynolds Creek stream (Figure 2.6) was examined for knickpoints. These knickpoints would explain disturbances or lithological changes within the landscape (Whipple and Tucker, 1999; Crosby and Whipple, 2006; Cook et al., 2013). Two significant knickpoints are present within the total longitudinal profile of Reynolds Creek stream. A topographic profile of Reynolds Creek stream with terrace elevations mapped to the profile (Figure 2.6). The terraces are based on each individual landform, and was produced to show if knickpoint propagation is related to the incision history of the landscape from the terraces. The topographic profile does not show a correlation between the terrace treads and the knickpoints.

2.5 Discussion

2.5.1 Geochronology

2.5.1.1 U-Th-Pb

Analysis of the LA-ICP-MS has shown interesting results in comparison to the type of ash present at the sample sites. Both samples that were found at the Pinnacle location were robust in zircons and ideal for analysis. The Quarry sample was noted as being a particularly dirty sample with lots of impurities. These impurities can be explained through the stratigraphic column, as the sample is found stratigraphically above a coal deposit. On the outcrop, this deposit has a yellowish hue to it, likely from the sulfur from iron deposits that washed onto the sample. The Quarry also appears to lack zircons, having 31 zircons compared to 57 in the Pinnacle samples. The Summit location has a two large peaks present within the sample, with a large Late Cretaceous inheritance that is not accounted for in any other sample. At the Summit location, the ash appears to be interbedded and reworked with the Arkosic unit. Because the Arkosic unit is derived from the underlying Cretaceous granite, that would explain the Late Cretaceous peak found in the Summit location samples. Based on the reworked nature of the Summit location ash, it shows the water or slope movement was occurring in this northeastern portion of the basin.

The data attempts to explain the mechanism for deposition based on the timing of the U-Th-Pb dates. Three hypotheses have been proposed: (1) Spillover from Lake Idaho sediments resulting in conditions able to accommodate a lacustrine environment, (2) Damming from the Rhyolitic lava flow of Reynolds Creek resulting in a lacustrine environment, and (3) regional extension resulting in subsidence that created a structural basin. The data appears to support hypothesis #2. Since the zircons are dated between 10.4 to 11.2 Ma, this rules out the possibility that these sediments were deposited in Lake Idaho. This does not rule out the possibility of structural deformation, though it is not supported by the topographic locations of the sediments nor the dates, this does not suggest that the scenario mentioned matches up with this scenario.

The data within our stratigraphic columns also correlates timing within the stratigraphic columns, as seeing that the lowest most ashes from the Quarry (Q1) and the Pinnacle (P1) were deposited within three thousand years of each other (Figure 2.7). Following the stratigraphy of the stratigraphic columns, it is likely that P3 correlates with the upper most ash present within the Quarry location. The Summit location's upper ash may possibly correlate with the Pinnacle and Quarry columns, though is not clear based on the data present.

Source potentials for the ashes are tough to nail down as during this time, volcanic activity was common in southwestern Idaho due to subsidence of the western Snake River Plain and the presence of the Bruneau Jarbridge Yellowstone hotspot track moving through the region

(Woods and Clemens, 2002). A location is proposed as possible sources for the ash (Mark Schmitz, per comm., 2021). A 2004 study found that the Cerro el Otoño Dome Field has an Ar-Ar date for the flow around 11.03 Ma (Bonnichsen et al., 2004). Given the source area of this ash, it is entirely possible for this ash to fall into the basin area (Figure 2.8).

2.5.1.2 OSL

The hypothesis for terrace abandonment is that terraces would date to early Quaternary in age. The ages are quite young, with Qt4 and Qt3 both being dated around 25-30 kya. These dates reject the hypothesis that the ages of the terraces would be early Quaternary, as they are late Quaternary in age. These ages do match with other terraces within the western Snake River Plain.

The ages presented within the OSL section shows the oldest terrace sample, Qt4, being about 1,000 years older than the sand lense deposit found at Qt3. Furthermore, the loess deposit within Qt3 was dated to be 8,000 years younger than the loess sample within Qt3. The dates are all within two standard deviations of one another, with an overlap around 25.3 kya. I conclude from the data that the burial age for these sediments were rapid and occurred at latest around 22 kya. The OSL data could not capture the individual timing of the terrace as the stream incision and abandonment rate was significantly faster than otherwise.

The terraces were mapped onto a longitudinal profile to see how these terraces stacked in long profile view, and if their incision/abandonment correlated with knickpoints found within the streams. The hypothesis for the terrace and knickpoints is that some of the older terraces would inflect an incision event that relates to the presence of the knickpoint. Recreating the stream profile from the knickpoint did not show any incision within the landscape that correlates to these knickpoints. Terrace incision into the landscape was a younger event, and occurred relatively recently when compared to the knickpoints.

2.5.2 Topographic Evolution

2.5.2.1 Overview

Using observations and data acquired from LiDAR mapping and ground-truthing, geochronology, and topographic analysis, I reconstructed the inferred topographic evolution of RC. The topographic evolution will be accompanied by multiple figures in part that help correspond with the current step in the topographic model. Each interpreted set has three elements: (1) a cross sectional view of Reynolds Creek stream based on the topographic analysis, reworked to create the appropriate stream profile at each given stage of the evolution, (2) a top down view of the basin map that shows what units are present where at given points within the evolution of RC, (3) the CoMU from the surficial geologic map that is used to help guide timing of the topographic evolution based on the units. The surficial geology will go from around 15 Ma to present day topography, and possible predictions of what will be seen in the future.

2.5.2.2 Volcanic Mantling

RC's evolution begins with an uneven exhumation of granitic bedrock. The exhumation can be assumed uneven through the presence of stream channels that later volcanic units would follow and deposit into (McIntyre, 1972). Exhumation of the granitic bedrock occurred up until around 36 mya (Benford et al., 2010). The first major event in the topographic evolution is the mantling of volcanic units throughout the landscape (Figure 2.9 and 2.10). The mantling of these events occurred in pulses beginning at 30.9 mya with the deposition of the Salmon Creek porphyritic olivine basalts, but has most of its deposition occurring between 15 to 12 mya (Norman et al., 1986). Mantling of these volcanic units occurred on pre-existing stream channels, such as the latite units with the volcanics. These volcanic units would create massive geologic structures throughout the basin, as seen in particular with the cuestas present on the eastern side of the basin.

Pulses of these mantlings have an origin in regional crustal extension within the landscape (McIntyre, 1972; Ekren et al., 1981; Bonnichsen et al., 2004). The cause for the regional extension is unclear, with some possibilities being the relation to structural deformation associated with the onset of the western Snake River Plain, or with the extension from the Idaho-Oregon Graben systems fault mechanism into Reynolds Creek (Woods and Clemens, 2002; Hooper et al., 2002).

2.5.2.3 Lacustrine Mechanism

The mechanism for the lacustrine processes is likely the damming of RC by the Rhyolitic lava flow of Reynolds Creek. This explains the onset of the lacustrine process, but does not explain the amount of filling or the overall process of filling. Based on the data collected from the stratigraphic columns, filling was not a quick process. Presence of fissile terrestrial clay in both the Pinnacle location and the Quarry location indicates some sediment deposition in areas that are near shore to land. Diatomaceous clay found within the sections were identified as still water sediments. Sediments within the Pinnacle location and the Summit location suggest that the still water was present in the basin between around 11.127 Ma to around 10.986 Ma. Small ash beds are deposited within the basin, with a majority of the column being dominated by diatomaceous clay material. Onset at this point indicates that the height of the water was at maximum 1260 meters above sea level.

The estimate of 1260 meters above sea level provides significant structural information for the Quarry location, as the elevation of the quarry sample, dated at 10.983 Ma, is only at 1200 meters above sea level. The sediments present beneath the ash layer are terrestrial clay deposits, implying that the environment here and at the pinnacle represents two different environments occurring simultaneously. Three options could explain the deviation in environment: (1) fault movement within the basin that moved the Quarry location below the Pinnacle location, (2) the Quarry location had a localized influx of terrestrial sediment based on pre-existing topography, or (3) the basin had a high sedimentation rate. No clear evidence of faulting was found when observing the LiDAR, likely resulting in the localized influx of terrestrial sediment to the quarry location based on pre-existing topography of the area. The source of this terrestrial sediments is unclear. A reasonable assumption is that they were derived from the Salmon Creek porphyritic olivine basalts. This interpretation is reasonable based on comparing the current topography of Reynolds Creek and the distance between the Quarry and the Salmon Creek porphyritic olivine basalts in the upper basin.

After the initial filling of the basin to 1260 meters above sea level, small gradual burst would occur until maximum fill height was reached. In the Pinnacle location, this change occurs around 15 meters higher, with the presence of an overlain by a paleosol. The paleosol would represent the unit reaching the surface before more influx of water occurred. The timing for the paleosol is unclear, but must be between 10.986 mya to 10.366 mya, which would constrain the time between the first and second sample found within the Pinnacle location. Above the paleosol, the shift occurs to more rapid influx of terrestrial clay sediments within the deposit, with small pockets of diatomaceous material appearing near the very top of the outcrop (around 20 meters from the top). This could imply that the deposition of the material reached a transition point between subaqueous deposition to subaerial deposition during the deposition of these units. The change from subaqueous to subaerial would be a temporary change, as it would not explain the maximum fill level of the Sedimentary Fill of Reynolds Creek, which is seen almost 50 meters above the pinnacle locality. Delta lobes are not present in the lower part of the basin where they would be expected. The assumption is that the delta lobes had eroded away and are not within the geologic record. The model displays the how the delta lobes might have presented within the environment (Figures 2.11-2.14).

Orientation of the beds indicates future structural deformation within the unit resulting in dipping beds. The dip is variable in with a maximum of 25° NW and averaged 12° NW. The cause of the tilting is unclear, as the positioning of the beds would indicate that either (1) a normal fault is present just west of the maximum fill level of the Sedimentary Fill of Reynolds Creek or (2) a reverse fault is present right where the current Reynolds Creek stream is. Previous interpretations have inferred a fault being present within the center of the basin where the Reynolds Creek stream flows, but was inferred to be a normal fault with the downthrown side on the east. A normal fault was mapped on the western side of the basin with the downthrown side allowing for beds to be tilting towards the NW (Bonnichsen and Godchaux, 2006). The previous mapping effort also indicated that the fault was only inferred, and the timing of the faulting is never elaborated on. My conclusions involve the faulting occurring pre-volcanic mantling, but created a paleotopography that allowed for units to be deposited in the lower basin the dip towards the NW.

During this same timeframe, fluvial eroded granitic sediments began to be transported and placed within the lower basin. Whether that transport was from localized granite outcrops present within the lower basin, or from granite highlands with long transport paths that are relatively undisturbed is unclear. The deposition of the Arkosic Unit is present on much of the eastern side of the basin. These sediments are most likely syn to post-deposition of the Sedimentary Fill of Reynolds Creek, as it is often found reworked in or on top of those sediments.

2.5.2.4 Dissection of a Volcanic Landscape

Timing of the incision history within the basin is fairly unclear. Evidence that points to the incision history show that initial incision must have occurred between 10 ma to 30 ka, which marks timings of U-Th-Pb of the youngest ash tested and OSL of the oldest terrace tested. For this reason, understanding the history of dissection is unclear, and additional samples are being collected in hopes of answering the question. The mechanism for causing the dissection into the landscape is likely structurally related.

Several normal faults that trend east-west are documented within the Rhyolitic Lava Flow of Reynolds Creek. These faults can be seen on outcrop (Figures 2.15-2.16). The down-thrown sides of these faults result in decreases in elevation towards the Snake River, resulting in higher topographic relief for the stream to cut back into the basin. The fault activity for this fault began about 15 mya, but was still consistent up until around 9 mya (Woods and Clemens, 2002). These faults are likely the catalyst that resulting with incision into Reynolds Creek.

Water was leaving through the basin before in incision back into the current present day landscape. The maximum elevation that the lacustrine diatomaceous sediments are seen on the eastern side of the basins is around 1350 meters above sea level (Figure 2.13). The maximum elevation the Rhyolitic lava flow of Reynolds Creek is seen today is around 1405 meters above sea level. This elevation is observed near the vent that the flow came out of. It is likely that where Reynolds Creek stream is at today, that the Rhyolitic lava flow of Reynolds Creek was deposited at a lower elevation than what was previously seen. The lava flow at this location would likely be capping out at around 1350 meters, and suggests that the erosive tools have now exceeded or matched with the deposition tools in the landscape, and also that a significant output from the basin would be found somewhere near this elevation (Figure 2.14).

Incision into the volcanic landscape timing is variable largely through the amount of rhyolite that needs to be dissected within the landscape. The Rhyolitic lava flow of Reynolds Creek extends for around 8 kilometers to the northeast of the basin. As the faulting finished and offset the rhyolite, incision cutting back would begin (Figures 2.15-2.20). The incision of the landscape would most likely be present at plains of weakness, in particular with the contact between the Rhyolitic lava flow of Reynolds Creek and the Cretaceous granite. This assumption remains true for the majority of the canyon output, as when observing the inside of the canyon granitic rock can be found to the west of the stream and rhyolitic rock is found the east. This incision process also requires a large influx of water, and paleoclimate of the region is sparse, but it likely was slowed through the presence of paleolakes present just outside of Reynolds Creek, such as Lake Idaho and Glenns Ferry Lake. These lakes would increase the baselevel for which the streams are flowing into, decreasing the erosion tools for the landscape. Glenns Ferry Lake, the later of the two lakes, began decrease in filling around 2 mya (Woods and Clemens, 2002). The draining of the lake would present an opportunity for the erosive properties of Reynolds Creek stream to cut into the rhyolite faster and present us with the present landscape.

2.5.2.5 Quaternary Processes

While initial incision is unclear, it is likely that incision into the basin occurred at a relatively rapid pace. This suggests that the overall incision that occurred in the basin is fairly young. Future OSL dates are being obtained from the older noncontiguous terrace to constrain incision timing.

Looking on the map while comparing with the longitudinal profile, two pronounced knickpoints are present within the lower basin. The first of those knickpoints (Figure 2.6) is located right at the outlet into the canyon, suggesting that the knickpoint is based on erosion that occurred from the faulting of the Rhyolitic lava flow of Reynold Creek. The second pronounced knickpoint appears just outside the lower basin. Initially, I hypothesized that this knickpoint is heavily related to the early stages of incision into the lower basin. Upon investigation, the knickpoint corresponds with an alluvial floor and landslide that occurred within the upper basin. This knickpoint is a response to the landslides that blocked the stream, and created an epigenic gorge to circumvent the blockage. An epigenetic gorge is created when a stream is laterally displaced after a disturbance in the landscape, either a blockage or rapid incision, blocks the current output of the stream (Ouimet et al., 2008). This was determined through the LiDAR and the presence of bedrock exposure throughout the location.

Seven distinct terrace are present within the region. Each of these terrace sets are gently sloping. The non-contiguous terraces are present dominantly on the western side of the basin, with only one terrace present on the eastern side of the lower basin, suggesting that material on the western side had more resistant cap material and/or access to more streams. The cap rock for the western side is more andesitic or basaltic than cap from for the eastern side, which is dominated by basalt. The differences in lithology do appear negligible in marking the creation of a terrace, but the amount of cap and size is significantly greater on the western side than the eastern side. On the western side of the basin, the noncontiguous terraces are formed by the Sedimentary Fill of Reynolds Creek, while on the eastern side of the basin, the noncontiguous terrace is formed by the Arkosic Unit. I conclude that the preservation of the terraces is largely based on the presence of cap rock within the basin.

The late Quaternary incision of the basin was fairly gradual, and has distinct steps for which the cuts occur. These are correlated with the presence of the terraces (Figures 2.17-2.20). The cuts are fairly gradual in size, but are likely to have occurred rapidly and in quick successions based on the erodibility of the material. The contiguous terraces are made of underlying volcanic bedrock and a mix of the Arkosic Unit. The underlying volcanic bedrock within this region is welded tuff, which could explain the nature of paired terrace steps. Timing of the contingent terrace steps are rapid, and occur between 30 kya to present day.

Future evolution in the region should see that the landscape returns to steady state conditions with the knickpoints progressing to the channel heads assuming stasis in a non-static landscape. Further incision should be seen within the lower basin in the future, though the rate at which this occurs is dependent on the stream path, climate, and underlying material, which cannot be accounted for as of now. Landslides will continue to affect the basin, but no large scale landslides are foreseen that would disturb the landscape to enter into a new steady state condition.

2.6 Tables

Table 2.1: U-Th-Pb ages

Sample Number	LA-ICP-MS age (my)	CA-ID-TIMS age (my)
P1	10.70 ± 0.18	10.986 ± 0.009
P3	10.62 ± 0.23	10.366 ± 0.009
S1	10.98 ± 0.36	11.127 ± 0.008
Q1	10.69 ± 0.36	10.989 ± 0.027
Rhyolite	n/a	11.413 ± 0.006

Table 2.2: OSL ages

Sample Number	USU number	Depth (m)	Number of Aliquots	Dose Rate (Gy/kyr)	Equivalent Dose ± 2σ (Gy)	OSL age ± 2σ (ka)	Terrace
RC Trench 1-1 (Sample #1)	USU-3457	1.8-1.9	16(32)	2.51 ± 0.11	75.42 ± 10.24	30.02 ± 4.76	Qt3
RC Pit 1-1 (Sample #2)	USU-3458	~1	21(31)	2.43 ± 0.10	54.16 ± 6.88	22.30 ± 3.37	Qt3
S01RCCZOLM (Sample #3)	USU-3464	3.5	19(35)	2.26 ± 0.09	65.70 ± 8.23	29.09 ± 4.35	Qt4

2.7 Figures

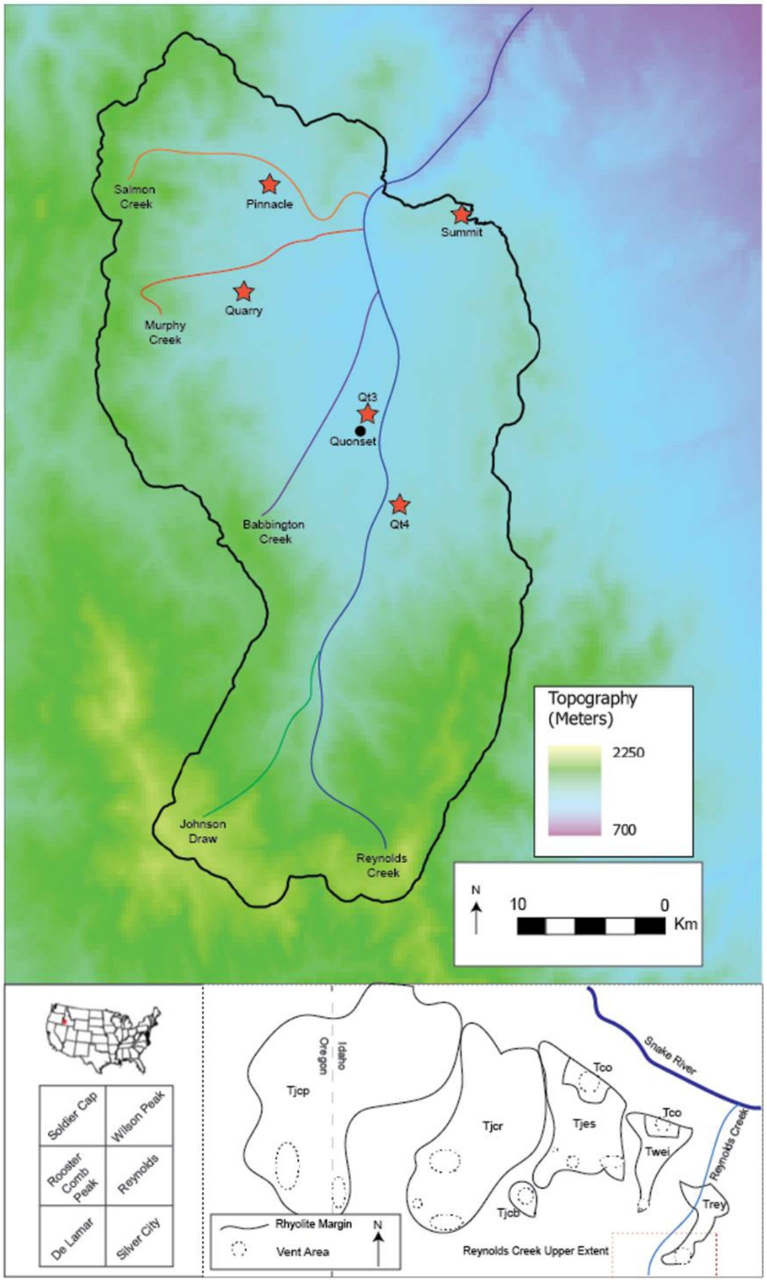

Figure 2.1: DEM of Reynolds Creek, Idaho. Names of major tributaries, sample localities, and reference locations are marked on the map. The US map and the USGS quads mark where Reynolds Creek is, and a regional rhyolitic geologic context map is placed to give context. The units are: (Trey) Rhyolitic lava flow of Reynolds Creek, (Tco) Rhyolite of the Cerro Otoño type, (Twei) Wilson Creek ignimbrite, (Tjes) Snare Snout Segment, (Tjcb) Share Snout segment, (Tjcr) Rockville Segment, and (Tjcp) Pole Creek Top segment

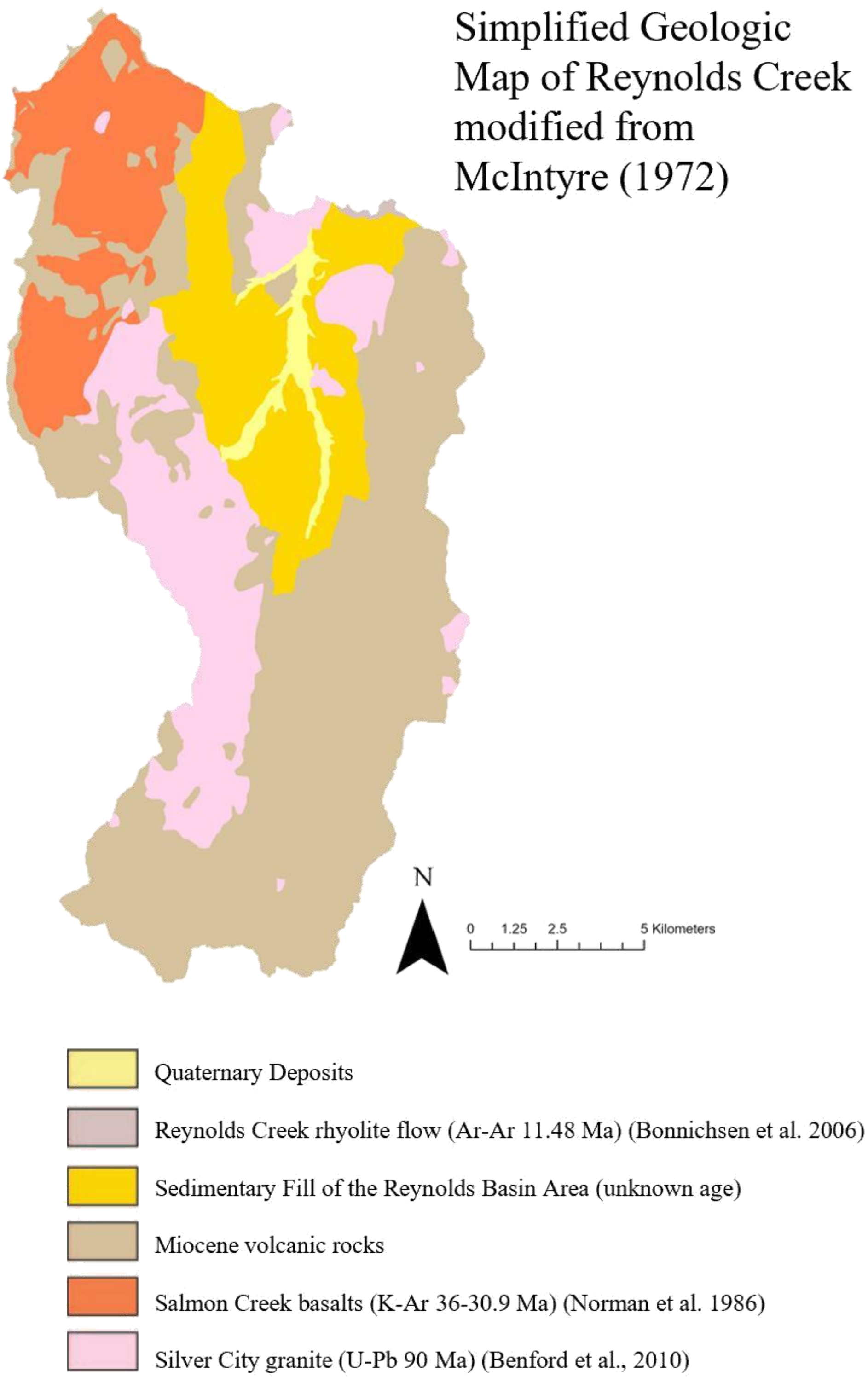

Figure 2.2: Simplified geologic map of Reynolds Creek. Modified from McIntyre (1972) to match unit names from Bonnichsen and Godchaux (2006).

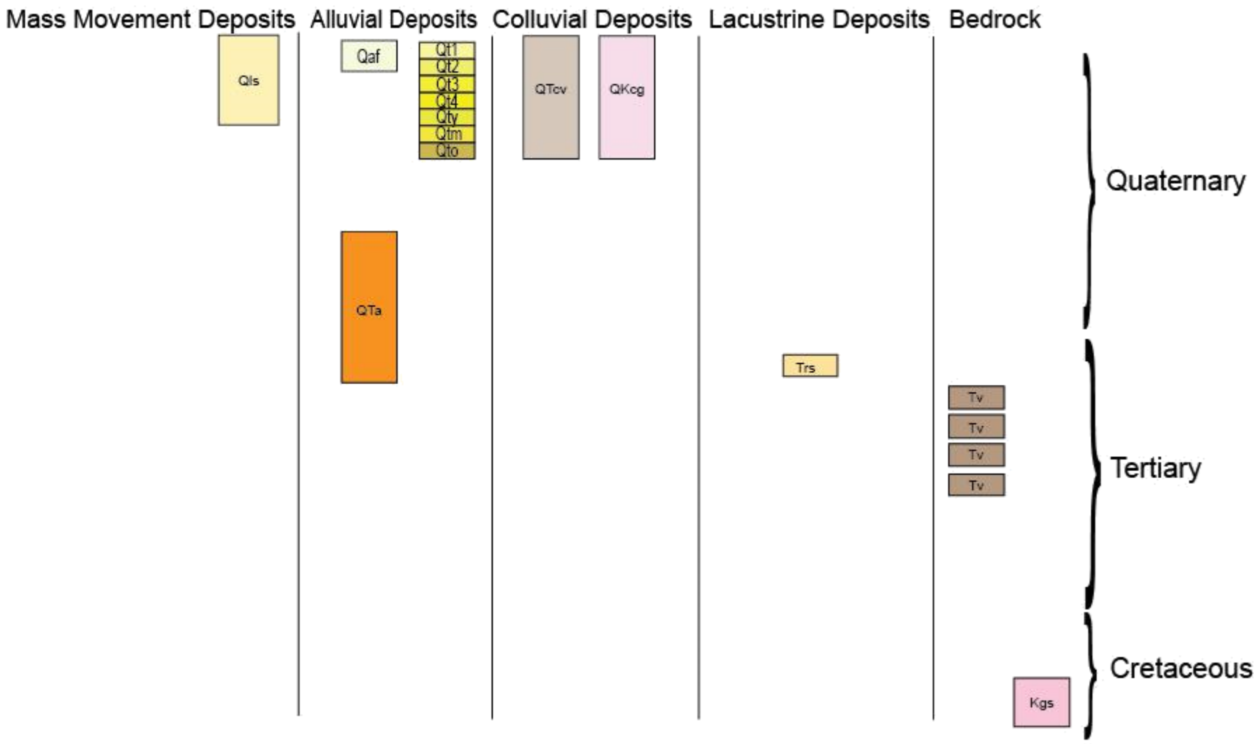

Figure 2.3: Correlation of Map Units for the surficial geologic map. The units are: (Qls) landslides, (Qaf) Alluvial floor, (Qt1) youngest contingent terrace, (Qt2) mid-young contingent terrace, (Qt3) mid-old contingent terrace, (Qt4) oldest contingent terrace, (Qty) Younger Terraces, (Qtm) Mid Terraces, (Qto) Older Terraces, (QTa) Arkosic Unit, (QTcv) Volcanic colluvium, (QKcg) Granitic colluvium, (Trs) Sedimentary basin fill of Reynolds Creek, (Tv) volcanic bedrock, and (Kgs) granitic bedrock

Figure 2.4: Outcrop of the Cuesta, located just east of the ARS station. Bedding suggests a dip toward the NW. largely composed of felsic latite with small, vitrified layers.

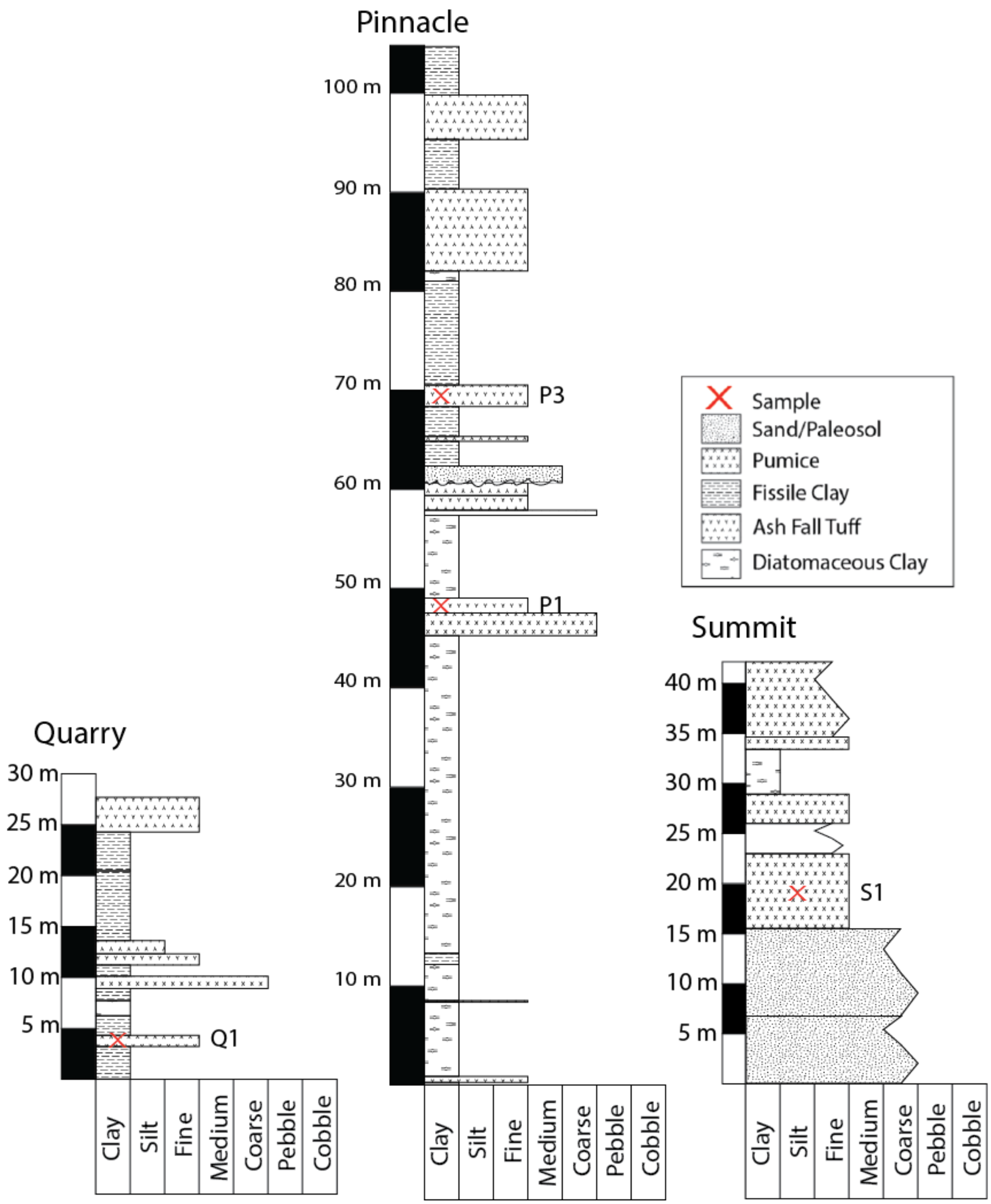

Figure 2.5: Stratigraphic columns of the Sedimentary Fill of Reynolds Creek. The three localities are labelled, along with their corresponding U-Th-Pb sample locations.

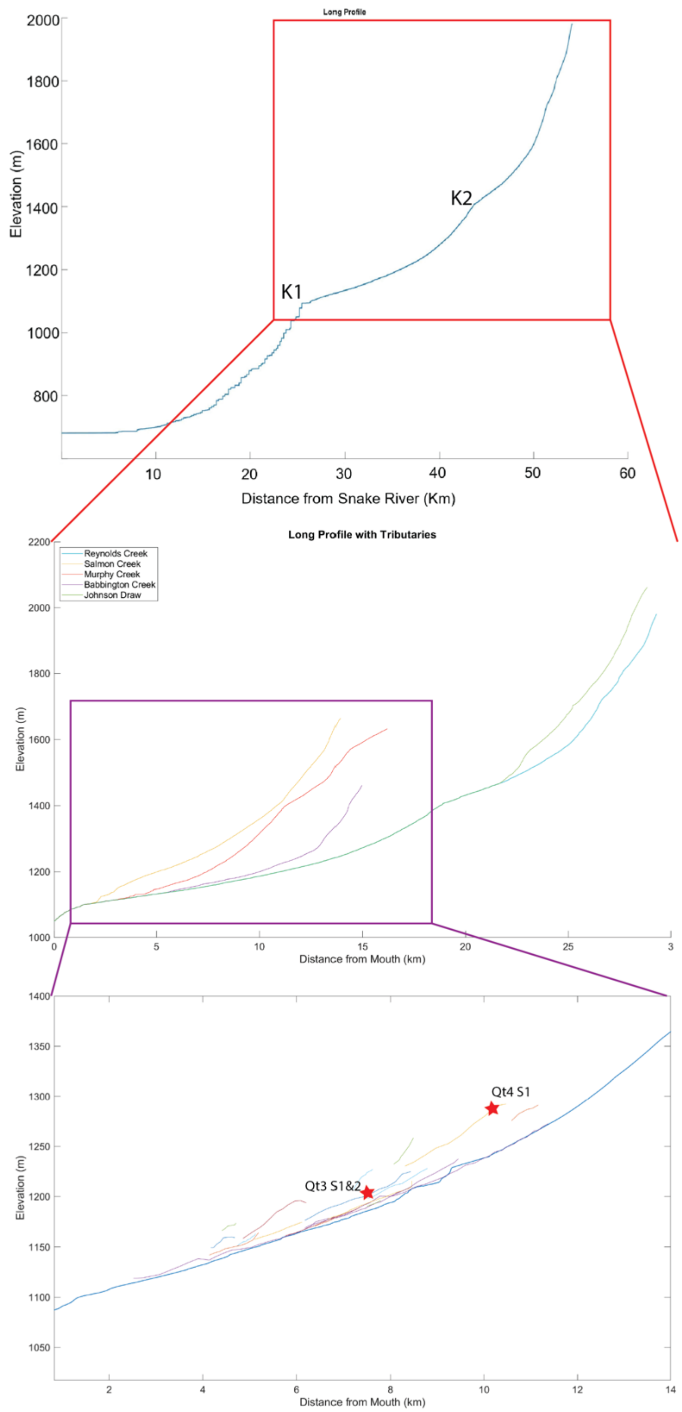

Figure 2.6: Topographic profiles of (1) Reynolds Creek to the Snake River, (2) Reynolds Creek with tributaries within Reynolds Creek and (3) Topographic profile within the lower basin with terraces elevations plotted. Terraces where OSL samples were obtained are marked on the profile.

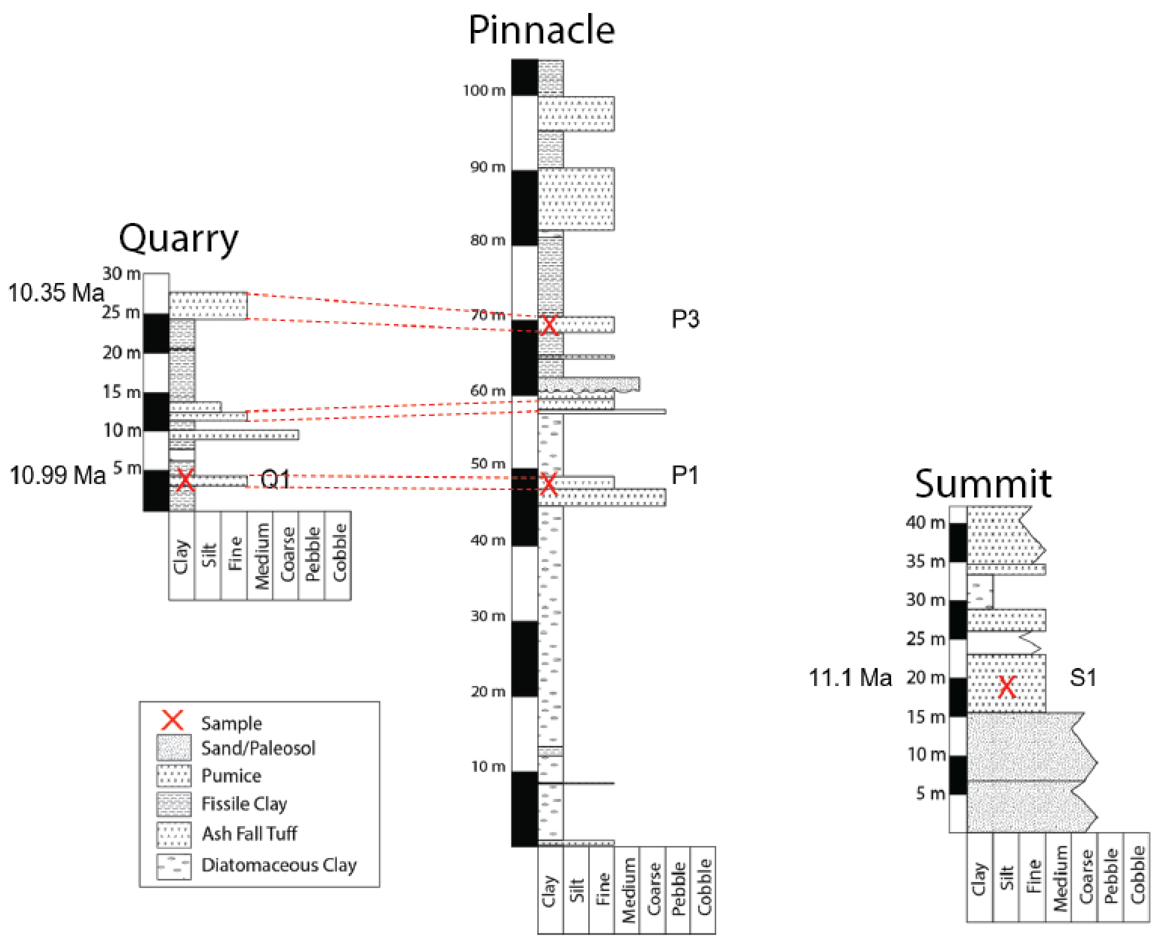

Figure 2.7: Correlated stratigraphic columns. Red lines represent the possible correlated ash beds.

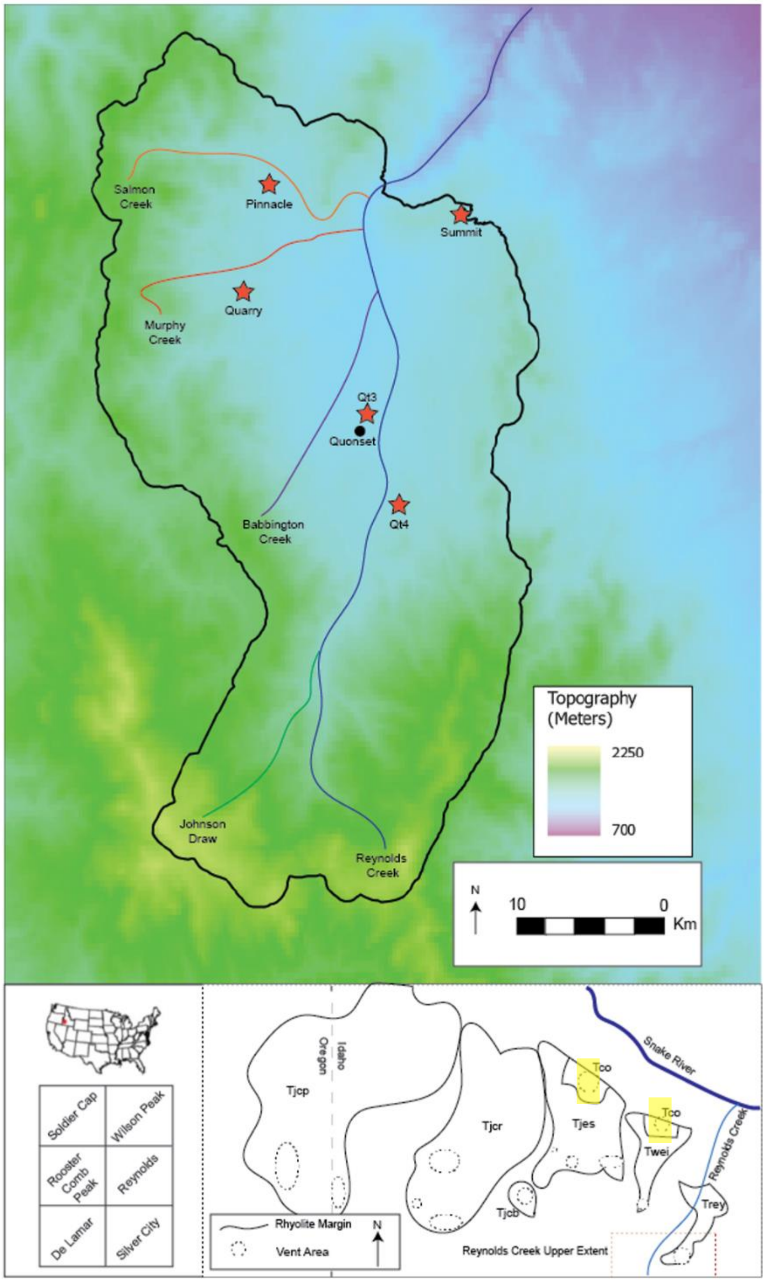

Figure 2.8: Overview DEM figure with the rhyolitic vents on map. The Cerro el Otoño vents are highlighted in yellow.

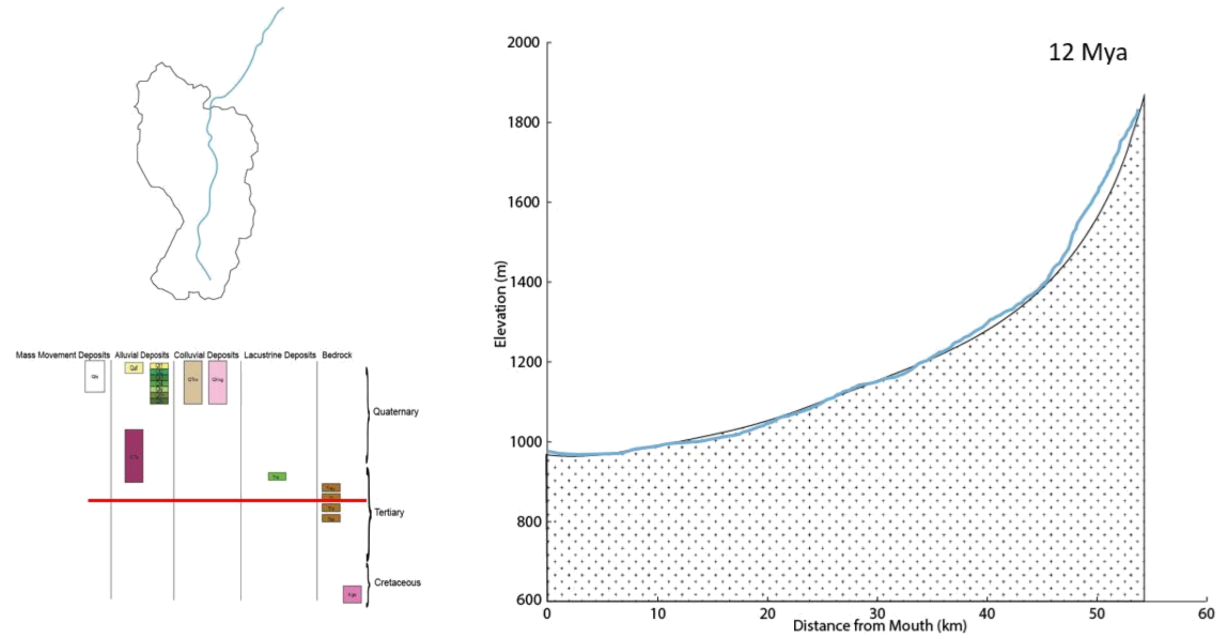

Figure 2.9: Topographic evolution model start, starting toward the end of the volcanic mantling. A stream profile is placed over top of the model.

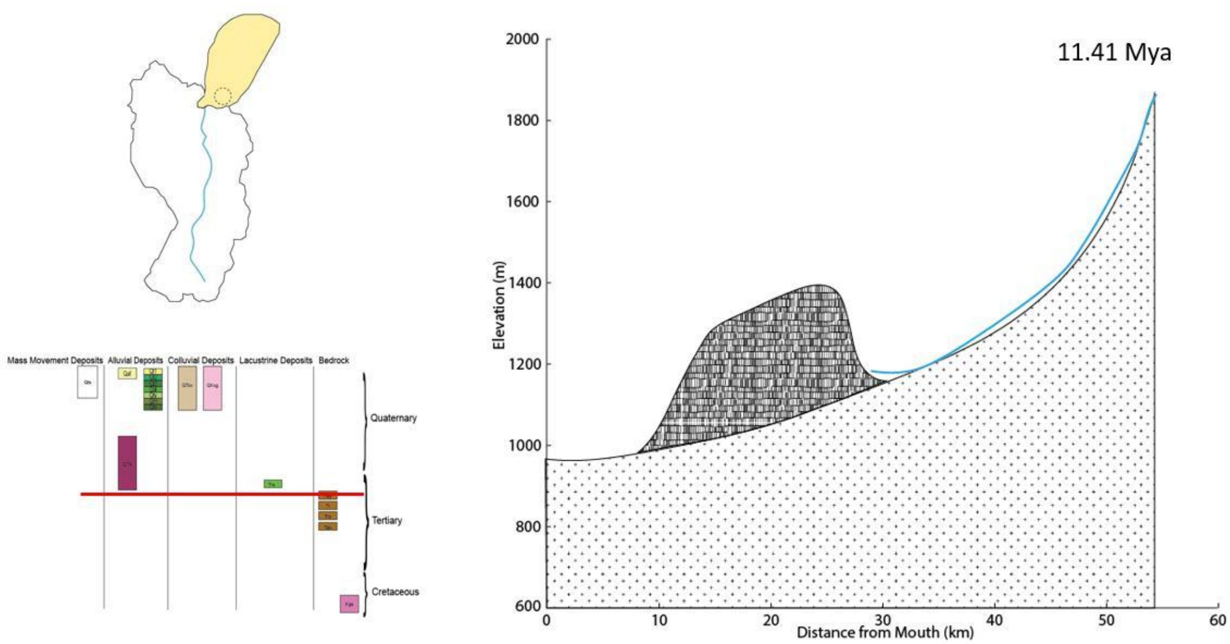

Figure 2.10: Topographic evolution model step 2, damming of the basin from the Rhyolitic lava flow of Reynolds Creek. Filling of the lake begins now. Timing based on U-Th-Pb dates obtained from the unit.

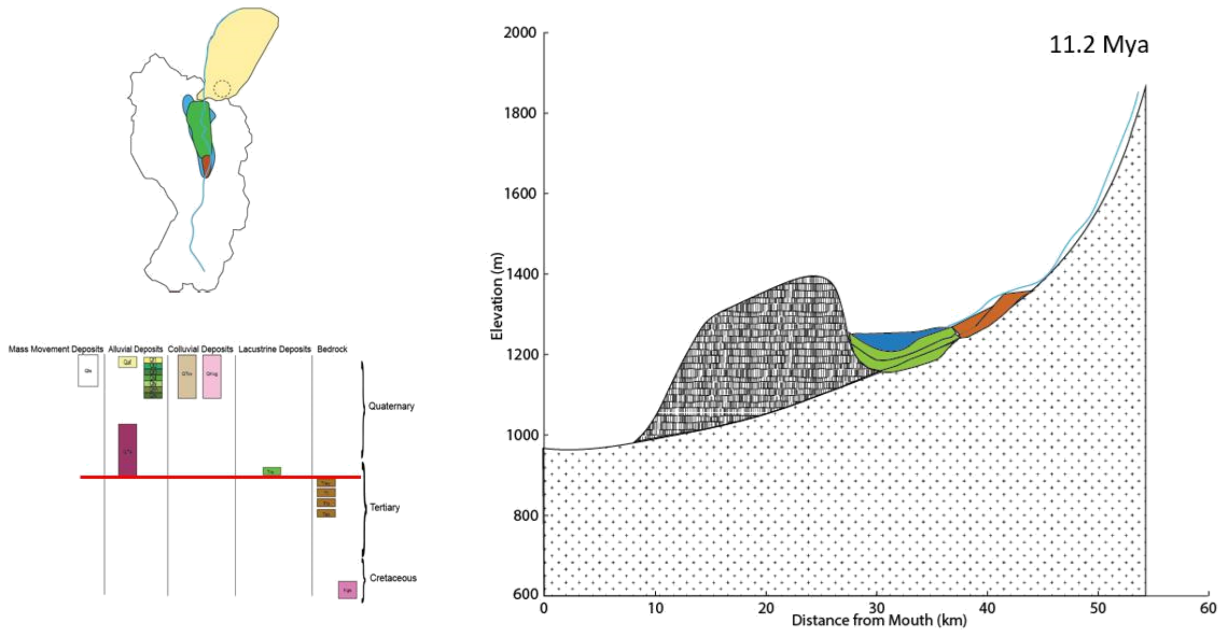

Figure 2.11: Topographic evolution model step 3, accumulation of lacustrine sediments along with filling. The sediments have a mix of lacustrine sediments along with terrestrial sediments, as seen within the stratigraphic columns.

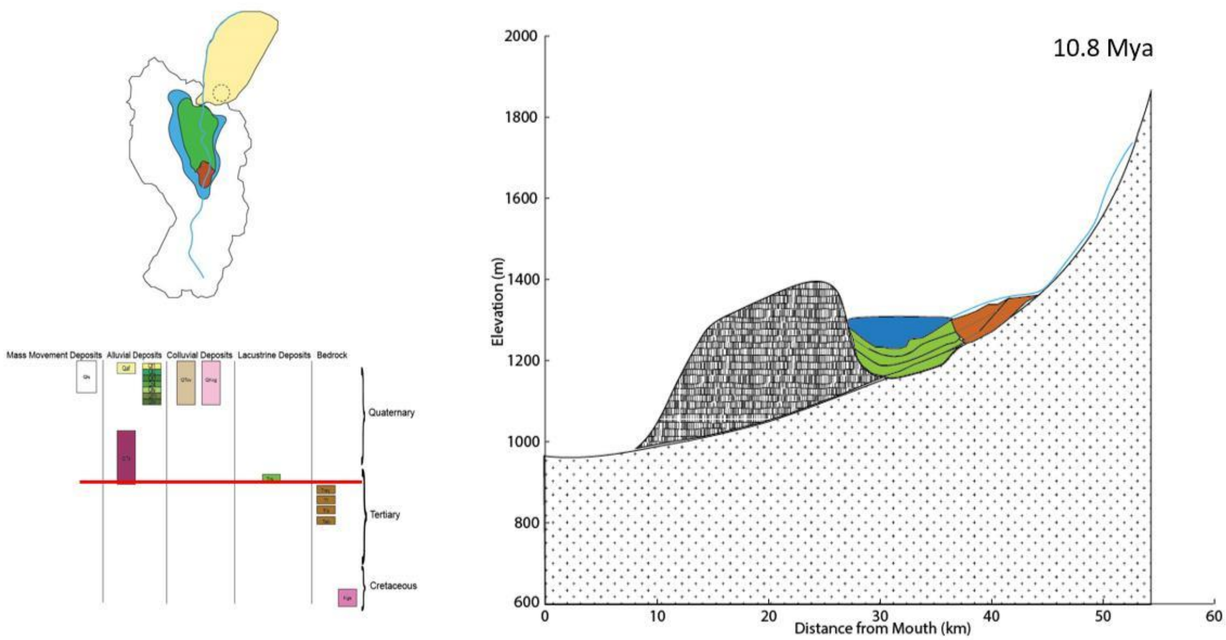

Figure 2.12: Topographic evolution model step 4, further accumulation. Following the same process seen within step 3

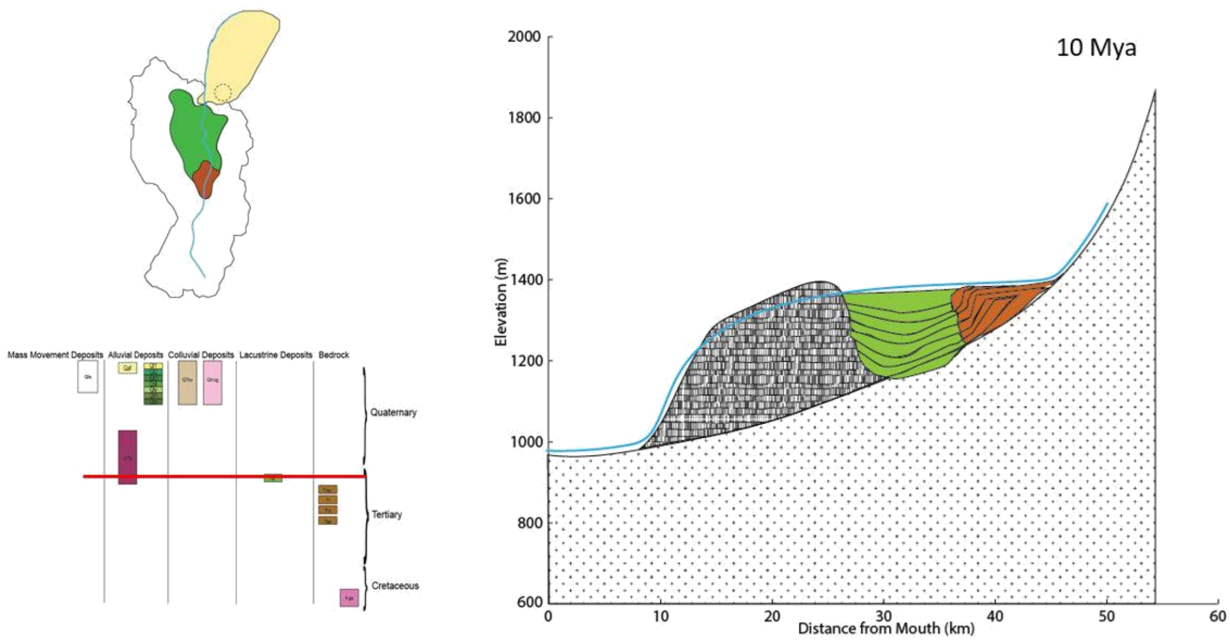

Figure 2.13: Topographic evolution model step 5, Filled basin. Timing based on U-Th-Pb samples. Height of fill based on DEM data from ground-truthing.

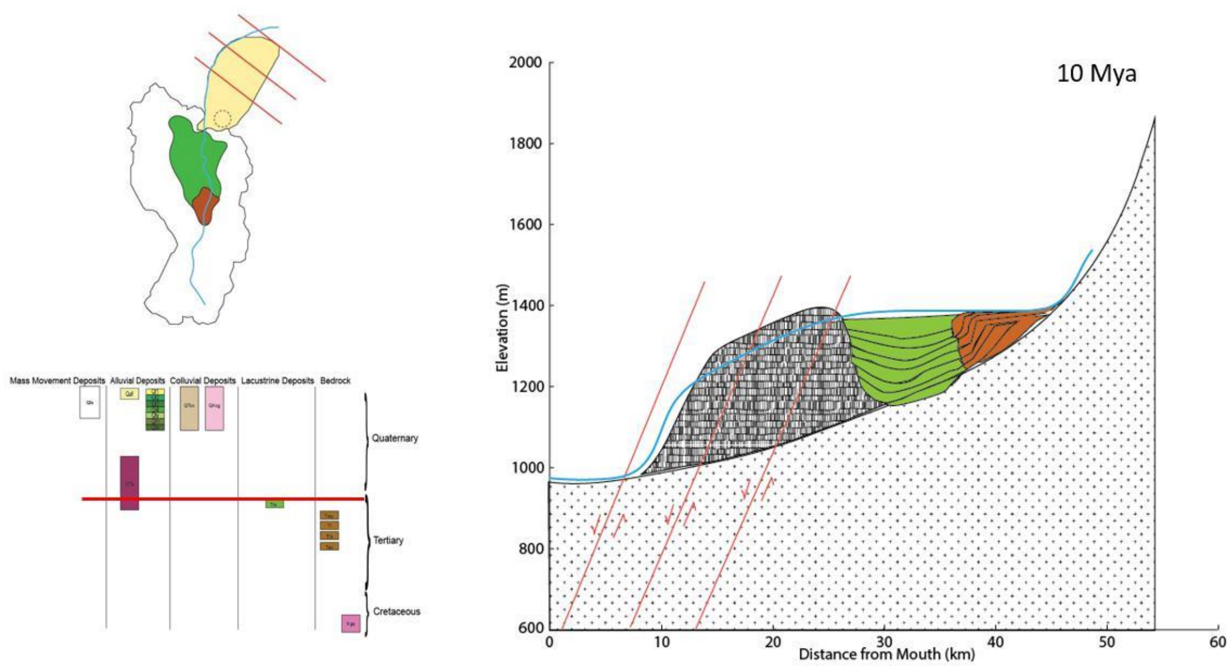

Figure 2.14: Topographic evolution model step 6, faulting occurring, this faulting can be observed within google earth imaging, timing based on Woods and Clemens (2002).

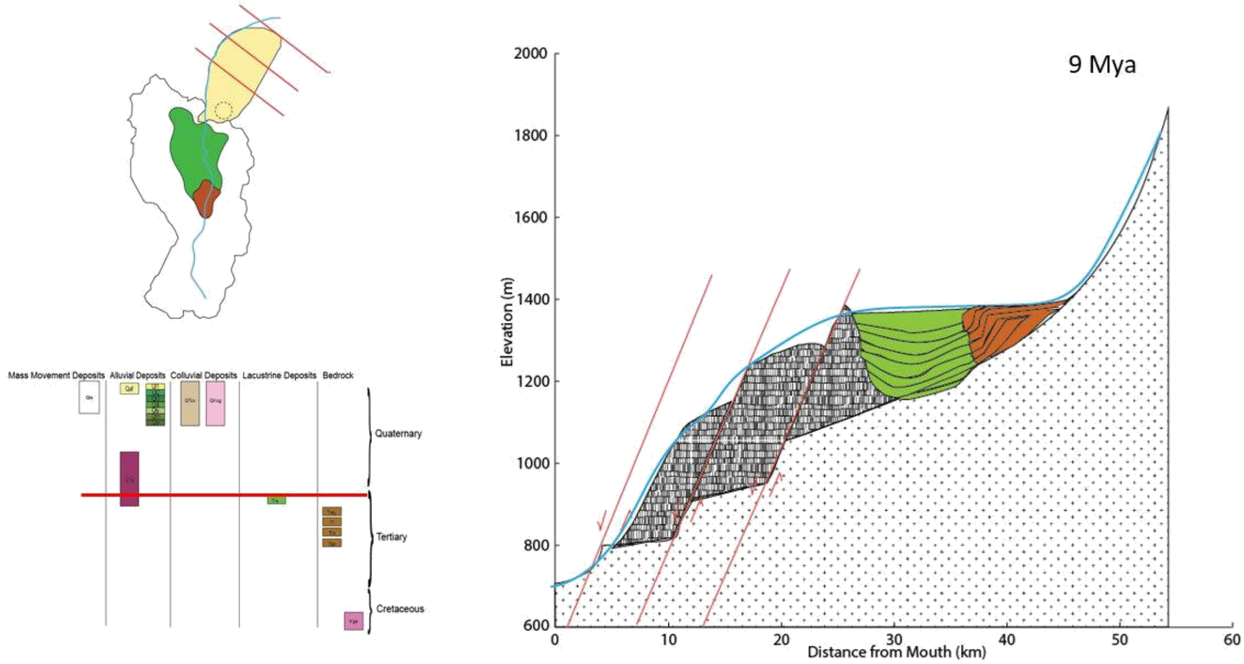

Figure 2.15: Topographic evolution model step 7, faulting movement. This faulting movement shows outlet to Snake River at the current location it is at.

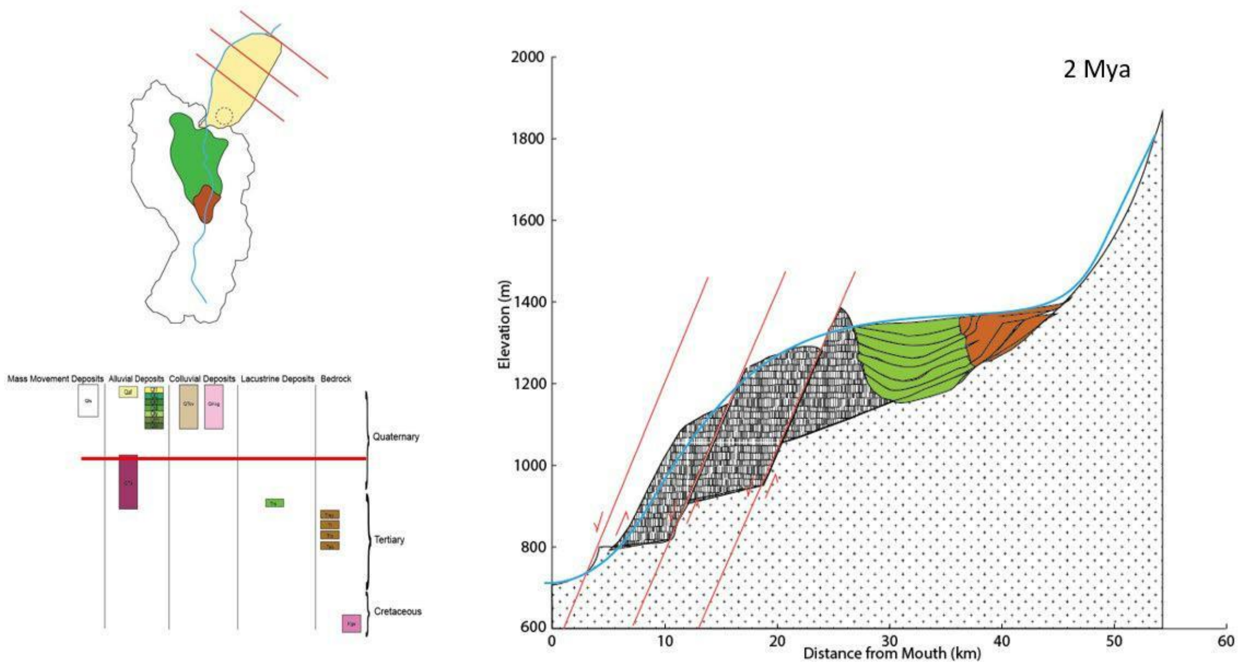

Figure 2.16: Topographic evolution model step 8: Incision beginning. Timing is unclear, and is largely based on the presence of young terraces for OSL.

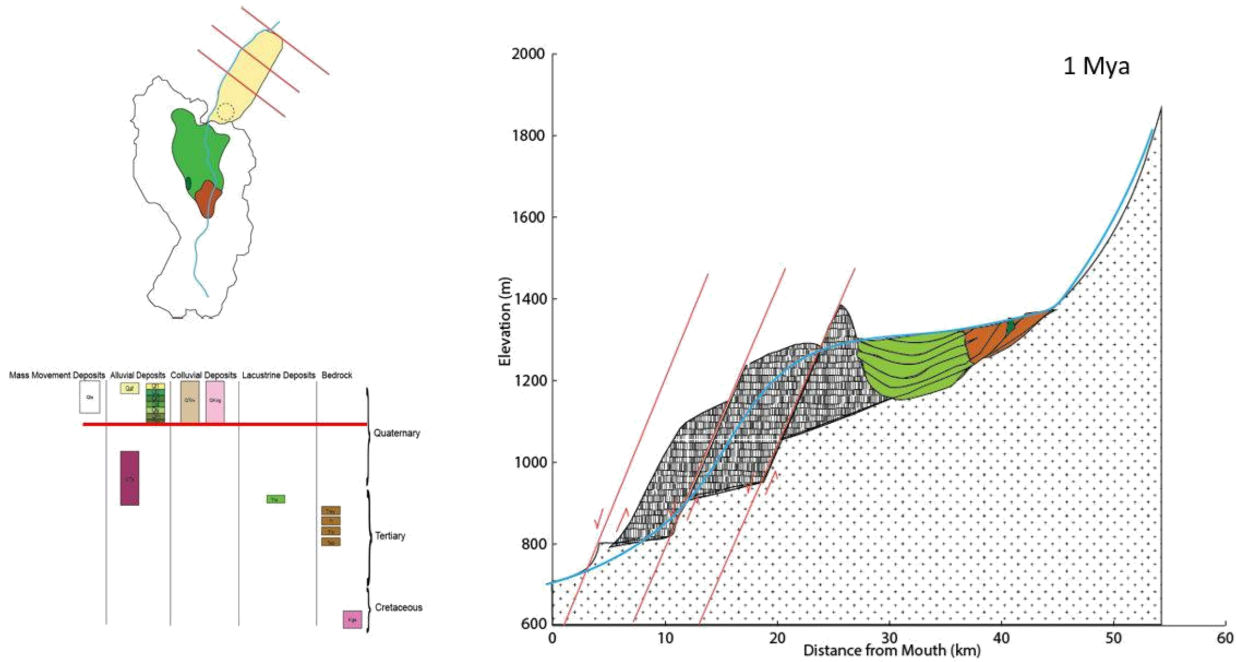

Figure 2.17: Topographic evolution model step 9: Further incision. Process cuts back into the Rhyolitic lava flow of Reynolds Creek along with cutting down in the basin. Remnants of activity are preserved in terraces.

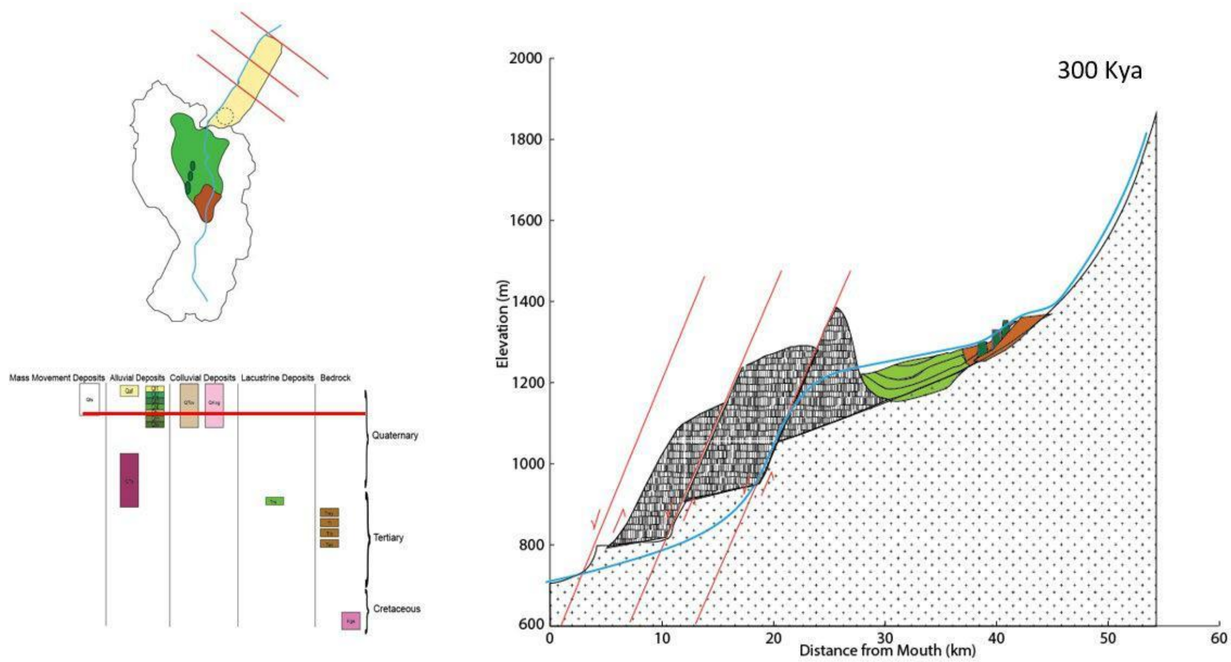

Figure 2.18: Topographic evolution model step 9: More incision, follows process similar to what was presented in step 8.

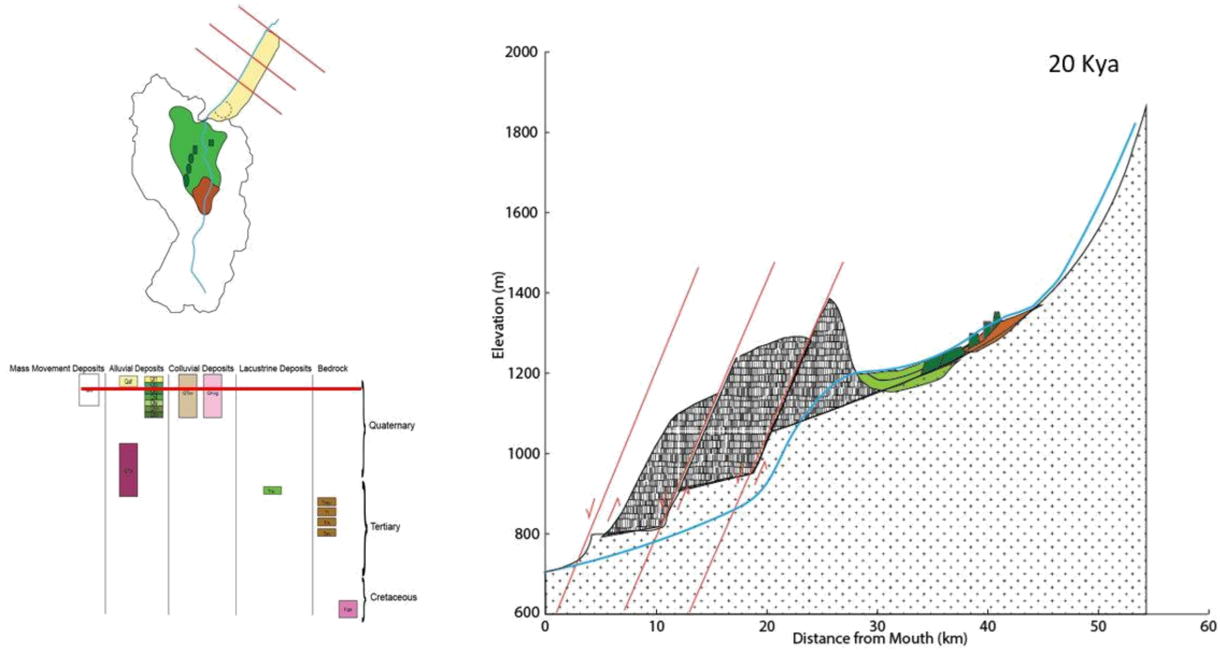

Figure 2.19: Topographic evolution model step 10: Even further incision, timing based on OSL data obtained from Qt3 and Qt4.

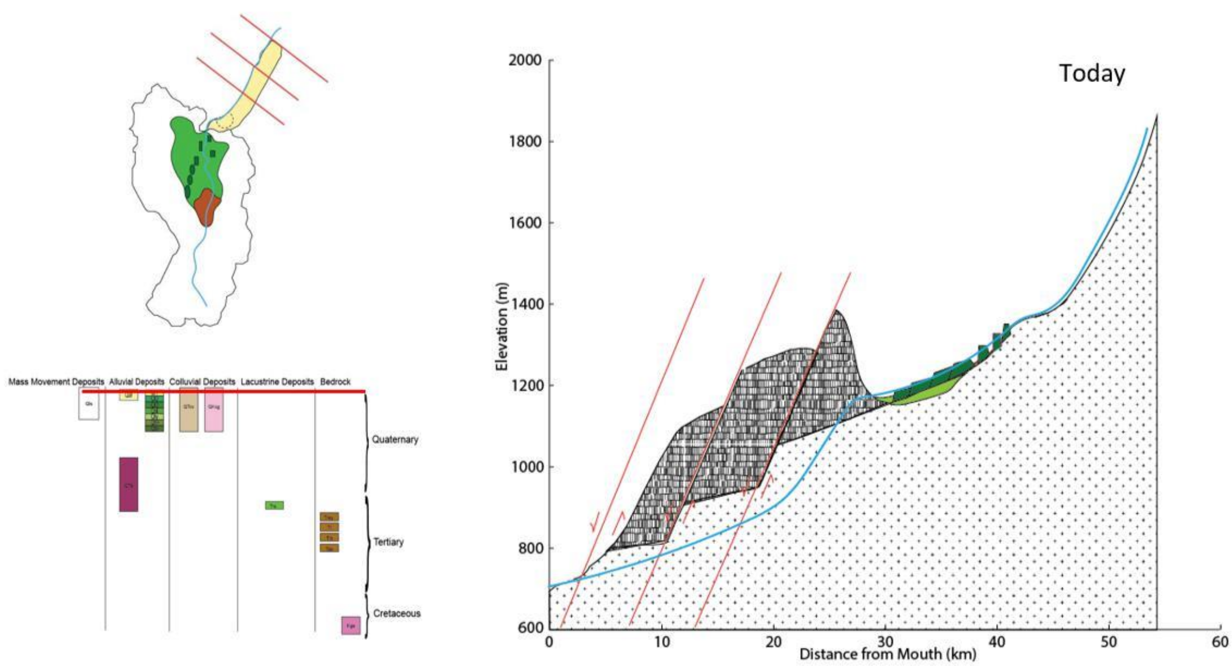

Figure 2.20: Topographic evolution model step 11: Today’s landscape, based on the overall longitudinal profile shown in Figure 2.22. Knickpoint present above a result of the landslide creating an increased alluvial floor within the region.

2.8 References

Aitken, M.J., 1998, An Introduction to Optical Dating: Oxford University Press, 276 p.

Allen, C.M., and Campbell, I.H., 2012, Identification and elimination of a matrix-induced systematic error in LA-ICP-MS 206Pb/238U dating of zircon: Chemical Geology, v. 332– 333, p. 157– 165

Anderson, S.P., Anderson, R.S., Tucker, G.E., 2012a, Landscape scale linkages in critical zone evolution: Comptes Rendus Geoscience, v. 344, no. 11-12, p.586-596, doi:10.1016/j.crte.2012.10.008.

Benford, B., Crowley, J., Schmitz, M., Northrup, C.J., Tikoff, B., 2010, Mesozoic magmatism and deformation in the northern Owyhee Mountains, Idaho: Implications for along-zone variations for the western Idaho shear zone: Lithosphere, v. 2, p.93-118, doi:10.1130/L76.1.

Beranek, L.P., Link, P.K., Fanning C.M., 2006, Miocene to Holocene landscape evolution of the western Snake River Plain region, Idaho: using the SHRIMP detrital zircon provenance record to track eastward migration of the Yellowstone hotspot: Geological Society of America Bulletin, v. 118, p. 1027-1050

Bonnichsen, B., Godchaux, M.M., 2006, Geologic Map of the Murphy 30 x 60 Quadrangle, Ada, Canyon, Elmore, and Owyhee Counties, Idaho: Idaho Geologic Survey Digital Web Map, no 80, scale 1:100,000

Bonnichsen, B., McCurry, M., Godchaux, M.M., 2004, Miocene Snake River Plain rhyolites of the Owyhee Front, Owyhee County, Idaho, Geological field trips in southern Idaho, eastern Oregon, and northern Nevada: U.S. Geological Survey Open-File Report 2004-1222, p. 154-173

Briant, R.M., Bates, M.R., Marshall, G.D., Schwenninger, J.-L., Wenban-Smith., F.F., 2012, Terrace reconstruction and long profile projection: a case study from the Solent River system near Southampton, England: Proceedings of the Geologists' Association, v. 123, p. 438-449

Brocard, G., Willenbring, J.K., Scatena, F.N., Johnson, A.H., 2015, Effects of a tectonically- triggered wave of incision on Riverine Exports and Soil Mineralogy in the Luquillo Mountains of Puerto Rico: Applied Geochemistry, v. 63, p. 586– 598

Camp, V.E., Ross, M.E., Duncan, R.A., Jarboe, N.A., Coe, R.S., Hanan, B.B., Johnson, J.A., 2013, The Steens basalt: Earliest lavas of the Columbia River basalt group, in Reidel, S.P. et al., eds., The Columbia River flood basalt province: Geological Society of America, Special Paper 497, p. 87–116

Cook, K.L., Turowski, J.M., Hovius, N., 2013, A demonstration of the importance of bedload transport for fluvial bedrock erosion and knickpoint propagation: Earth Surface Processes and Landforms, v. 38, p. 683– 695, doi: 10.1002/esp.3313

Crosby, B.T., and Whipple, K.X., 2006, Knickpoint initiation and distribution within fluvial networks: 236 waterfalls in the Waipaoa River, North Island, New Zealand: Geomorphology, v. 82, p. 16–38, doi: 10.1016/j.geomorph.2005.08.023

Ekren, E.B., McIntyre, D.H., Bennett, E.H., Malde, H.E., 1981, Geologic map of Owyhee County, Idaho, west of longitude 116 degrees W: USGS Numbered Series, no. 1256, scale:1:25,000, 2 sheets

Ellis, B.S., Schmitz, M.D., Hill, M., 2019, Reconstructing a Snake River Plain "super-eruption" via compositional fingerprinting and high-precision U/Pb zircon geochronology: Contributions to Mineralogy and Petrology, v. 174, no. 101

Flerchinger, G.N., Fellows, A.W., Seyfried, M.S., Clark, P.E., and Lohse, K.A., 2019, Water and carbon fluxes along an elevational gradient in a sagebrush ecosystem: Ecosystems, p. 1–18, https://doi.org/10.1007/s10021-019-00400-x

Forte, A.M., and Whipple, K.X., 2018, Short communication: the topographic analysis kit (TAK) for TopoToolbox: Earth Surface Dynamics Discuss, v. 7, p. 87-95

Godsey, S., Marks, D., Seyfried, M., Kormos, P., Enslin, C., Winstral, A., McNamara, J.P., Link, T.E., 2018, Eleven years of mountain weather, snow, soil moisture and streamflow data from the rain-to-snow transition zone: The Johnston Draw catchment, Reynolds Creek Experimental Watershed and Critical Zone Observatory, USA: Earth Systems Science Data, v. 10, p. 1207– 1216

Hanson, C. L., Marks, D., and Van Vactor, S.S., 2001, Long-term climate database, Reynolds Creek Experimental Watershed, Idaho, United States: Water Resources Research, v. 37, p. 2839–2841, doi:10.1029/2001WR000417.

Hooper, P.R., Johnson, J.A., and Hawkesworth, C.J., 2002b, A model for the origin of the western Snake River Plain as an extensional strike-slip duplex, Oregon-Idaho, in Bonnichsen, B., White, C.M., and McCurry, M., eds., Tectonic and magmatic evolution of the Snake River Plain volcanic province: Idaho Geological Survey Bulletin 30

Hughes, P.D., 2010, Geomorphology and Quaternary stratigraphy: the roles of morpho-, litho-, and allostratigraphy: Geomorphology, v. 123, p. 189-199

Karlstrom, L., Richardson, P. W., O'Hara, D., Ebmeier, S. K., 2018. Magmatic landscape construction: Journal of Geophysical Research: Earth Surface, v. 123, p. 1710–1730

Lindgren, W., and Drake, N.F., 1904, Description of the Silver City Quadrangle: U.S. Geological Survey Atlas, v. 104, p. 1-4

Litchfield, N.J., Berryman, K.R., 2005, Correlation of fluvial terraces within the Hikurangi Margin, New Zealand: implications for climate and base-level controls: Geomorphology, v. 68, p. 291– 313

McIntyre, D.H., 1972, Cenozoic geology of the Reynolds Creek Experimental Watershed, Owyhee County, Idaho: Idaho Bureau of Mines and Geology, pamphlet 151, 115 p.

Nasdala, L., Lengauer, C.L., Hanchar, J.M., Kronz, A., Wirth, R., Blanc, P., Kennedy, A.K., Seydoux-Guillaume, A.M., 2002, Annealing radiation damage and the recovery of cathodoluminescence: Chemical Geology, v. 191, p. 121–140

Norman, M.D., McElwee, K.R., Duncan, R.A., and Leeman, W.P., 1986, K-Ar ages of Oligocene Salmon Creek volcanics. Owyhee Mountains, Idaho: Isochron/West, v. 46, p. 9-14

Ouimet, W. B., K. X. Whipple, B. T. Crosby, J. P. Johnson, and T. F. Schildgen, 2008, Epigenetic gorges in fluvial landscapes, Earth Surface Processes Landforms, v. 33, p. 1993–2009

Pierson, F.B., Slaughter, C.W., and Cram, Z.K., 2000, Monitoring discharge and suspended sediment, Reynolds Creek Experimental Watershed, Idaho, USA: ARS Technical Bulletin, NWRC-2000-8, 20 p.

Robins, J. S., Kelly, L.L., Hamon, W.R., 1965, Reynolds Creek in southwest Idaho: An outdoor hydrologic laboratory: Water Resource Research, v. 1, p. 407– 413, doi:10.1029/WR001i003p00407

Schwanghart, W., and D., Scherler, 2014, Short Communication: TopoToolbox 2 – MATLAB-based software for topographic analysis and modeling in Earth surface sciences, Earth Surface Dynamics, v. 2, p. 1–7, doi:10.5194/esurf-2-1-2014.

Seyfried, M., Lohse, K., Marks, D., Flerchinger, G., Pierson, F., and Holbrook, W.S., 2018, Reynolds Creek Experimental Watershed and Critical Zone Observatory: Vadose Zone Journal, v. 17, p. 1-20

Thouret, J.-C., 1999, Volcanic geomorphology—an overview: Earth-Science Review, v. 47, p. 95-131

Viveen, W., Schoorl, W.M., Veldkamp, A., Van Balen, R.T., Desprat, S., Vidal-Romani, J.R., 2013, Reconstructing the interacting effects of base level, climate, and tectonic uplift in the lower Mino River terrace record: a gradient modeling evaluation: Geomorphology, v. 186, p. 96-118

Warix, S.R., Godsey, S.E., Lohse, K.A., and Hale, R.L., 2020, Dataset for Flow Presence and Groundwater Fluxes at Murphy Creek, Southwest Idaho [Data set].

Wehrs, K.E., 2018, Interpreting River Incision History using Terraces and Mass Movements along the South Fork Eel River, Northern California [M.S. thesis]: Idaho State University, 115 p.

Whipple, K.X., and Tucker, G.E., 1999, Dynamics of the stream-power river incision model: Implications for height limits of mountain ranges, landscape response timescales, and research needs: Journal of Geophysical Research: Solid Earth, v. 104, p. 17661–17674, doi: 10.1029/1999JB900120.

Wintle, A. G., and Murray, A. S., 2006, A review of quartz optically stimulated luminescence characteristics and their relevance in single-aliquot regeneration dating protocols: Radiation Measurements, v. 41, p. 369– 391

Wood, S.H., Clemens, D.M., 2002, Geologic and tectonic history of the western Snake River Plain, Idaho and Oregon, Tectonic and Magmatic Evolution of the Snake River Plain Volcanic Province: Idaho Geological Survey Bulletin, v. 30, p. 69–103

Chapter 3: Conclusions

3.1 Synthesis

3.1.1. Volcanically Dammed Basins

RC falls in line with previously studied volcanic basin within both the western Snake River Plain and in the Grand Canyon (Fenton et al., 2002, Ely et al., 2012). Volcanic dams found in the Owyhee River, such as those created by the Bogus Rim lava flow or the West Canyon lava flow, created environments for lacustrine sediment deposition. These dams were at largest around 100 meters deep (Ely et al., 2012). In terms of size, RC is significantly larger than lacustrine environments caused by volcanic damming. Lake level within RC is at minimum 150 meters from base level based on mapping efforts, 50 meters higher than other basins in the region.

RC provides a unique prospective that the basin and damming occurred more than ten mya. Volcanic dams within the Grand Canyon and the western Snake River Plain all occurred within the last one million years. All of the basins do not present signals of damming within the longitudinal profile of the streams, with most signals believed to be unseen after a 10^4 to 10^6 timeframe. The signal losses present in the Grand Canyon are relicts of the dams failing, resulting in catastrophic flooding. This failure was caused from unstable slopes, fractured layers within the basalt flow, hydrothermal weaking of the flows, and tephra interbedding (Fenton et al., 2002, Crow et al., 2008). These catastrophic flooding events lead to increased transport of sediment into the Grand Canyon, resulting in further changes to the topographic evolution. In terms of the western Snake River Plain and RC, the volcanic damming was stable and was slowly eroded away through incision. The timing of this incision is unclear within RC, but with the Bogus Rim lava flow incision began after 1.7 mya and incised at a rate of 0.18 mm/yr (Ely et al., 2012). I can infer that RC has a much slower incision rate and timing of incision based on the timing of the damming and the presence of the knickpoint today. The longer incision rate is likely associated with the size of the dam. The volcanic flow has 200 meters to where the present day stream is located, and extends 20 km North/Northeast toward the Snake River. Relief on this slope was also relatively shallow based on the relief today and the overall fault throw that is present. Filling of the western Snake River Plain basins compared to RC is slightly different as well. Little to no lag time is present with the filling of the basin created with the Bogus Rim lava flow, filling fairly rapidly. Compared to the U-Th-Pb dates retrieved from the ashfall deposits in RC, filling took place over at least one million years. Factors for the rate may include the size of the basin, the overall climate of the basin, and the susceptibility for the water to remain still for deposition. As seen in the strat columns, two distinct clays are present and are interpreted to represent the filling of the lake to have been considerable slow, with plenty of terrestrial clays filling into the basin.

It is evident that the effects of the damming shape the landscape. Within the longitudinal profile (Figure 3.1), the large knickpoint located in the middle of the profile shows a steep decline where the damming was at. These extrafluvial signals are present, and on magnitudes on the 10^7 year scale, which are significantly longer than what was concluded in Korup et al. (2010). It was concluded in other studies that these extrafluvial events dominate the basin evolution (Stock et al., 2005, Cheng et al., 2006, Pratt-Sitaula et al., 2007). RC is able to further push the idea that these extrafluvial events are the driving force for the evolution of the basins and persist for much longer than previously studied, including what is present within the western Snake River Plain.

Though not a dammed basin in the same way, many landscape blocked basins also show similar characteristics that are present within RC. Both prevent sediments from leaving, allow for rapid filling of the basin, and have the incision signals, but are significantly less stable than volcanic flows. For example, a study conducted by Safran et al. (2015) observed landslide dams in Oregon basins and their impact on the landscapes. Of the 17 landslide dams studied, only one has yet to be breached. Many of these landslides were classified as ancient and predicted to have occurred between 10^3 to 10^4 years ago. These landslide dam failures would lead to catastrophic flooding, which changes the future evolution of the basin with further initial transport and fast incision rates (Fenton et al., 2006).

RC does fall in line with many of the surrounding volcanically dammed basin within the western Snake River Plain. RC is more longstanding with the signals it shows, and shows that these signal may be present for the basins in the western Snake River Plain that are younger than it.

3.1.2. Landscape Evolution Model

A landscape evolution model has been created to better show the periods of transience and equilibrium are present within RC (Figure 3.2). Reynolds Creek begins at a fairly consistent equilibrium state around 16 mya. While there has been some volcanic deposition, most of the volcanic activity has not begun as of yet. These changes begin around 15 mya, with the various pulses building up basin. Little lag time is present, with the relaxation time occurring almost immediately as the flows occur. This changes the equilibrium environment to a higher elevation.

Once the lava flows are emplaced, the equilibrium lowers as the landscape adjusts to the new topographic highs to create a new landscape. Since the lava flows come in pulses, the movement of the graph is repetitive with a slight upward trend in elevation. During the last pulse, the basin is dammed by the rhyolitic lava flow. Lag time is measured to be at most 0.3 million years based on the U-Th-Pb timings of the ashfall and the rhyolitic flow. Elevation increasing on the graph is fairly rapid, and reaches a maximum at around ten million years.

Small oscillations in the graph remain present for millions of years based on the presence of the damming. It is unlikely that the damming is incised and lowered until the lower of both Lake Idaho and Glenns Ferry Lake, but minor changes are represented within the model for climatic differences that may have occurred before full incision. While no clear markers indicate this oscillation, it is unlikely that no geomorphic change occurred over the span of seven to eight million years. Once incision occurs into the landscape, the basin is evacuated rather quickly and in multiple iterative steps. These incisions leave behind terraces, leaving remnants of where the stream was once active. The diagram continues to strive toward the new equilibrium, which balances the sediment remaining in the basin with the overall slopes of the streams.

3.2 Future Works in Reynolds Creek

3.2.1 Loess Deposit Map

Loess deposits is beginning to become a more focal point of research within RC. Though few publications have been made that focus on loess deposition, only being noted about the characteristics in the annual RC reports, loess deposition is an area that is being explored within RC (Seyfried et al., 2018). Loess deposit map would help classify the areas that loess is found within RC, and could be used to potentially identify plains of weakness that landslides may occur at (Liu et al., 2018). The future work would be adding in an additional layer with the loess deposits on the surficial geologic map. The underlying material is dominantly the units presented within my surficial geologic map, but loess does mantle much of the landscape. The overlay would allow for easier tracking of loess deposits within the basin, and can be used to better understand the mechanisms as to why loess deposits within certain locations.

3.2.2 Linking Soil Types and Chemistries with Landforms

Soil chemistry and soil types are well known within RC, but have not had a basin wide study that compares where the soils were found and how they relate. The relation is largely defined by the state factors, which are five controlling variables that determines soil properties (Jenny, 1941). These state factors are time, biota, climate, parent material, and topography. The surficial geologic map can be used to put the soil types and chemistries into context with the overarching surficial processes, and can be used to help further define which state factors play a large role in the soil properties. The surficial geologic map describes the overall surficial sediment in the area, and helps describe the processes that lead those sediments to the current location (Daniels et al., 1971).

A particular focus within RC is looking into the distribution of soil inorganic carbon throughout the basin (Fellows et al., 2017; Stanberry et al., 2017; Flerchinger et al., 2019). The surficial geomorphic map can be used to find trends present within the soil inorganic carbon throughout RC. Understanding the link between surficial processes and soil throughout the basin will be vital to future research within RC.

Soil linkage could also be used on to explain the presence of landforms within the surficial geologic map. In particular, a focus on understanding the soil types that are present on the eastern and western sides of the basin could explain the presence of landforms on each side. The study can also explain the presence of the high plateaued surfaces are preserved where they were found at.

3.3 Conclusions

By using LiDAR mapping and ground-truthing, geochronology, and topographic analysis with TAK, I was able establish a topographic evolution of RC that occurred from 15 mya to today. The topographic model follows the following steps. First, exhumation and emplacement of granitic rock that is then mantled by pulses of volcanic flows that are deposited in previous river channels. Next, the Rhyolitic lava flow of Reynolds Creek erupts and dams the basin, which creates an environment for which lacustrine deposition can occur. The Sedimentary Fill of Reynolds Creek fills in the accommodation space with the basin, with water filling in the basin at gradual steps. The fill contains both terrestrial clays that are sourced from an upland area and from diatomaceous clay when still water is present within the basin. This fill continues to fill until it reaches 1350 meters above sea level, where a large enough outlet for water to leave the basin provides a balance between the depositional and erosional tools required to prevent future deposition past this height. Faulting occurs within the Rhyolitic lava flow of Reynolds Creek, resulting in incision headed back towards Reynolds Creek. Gradual incision occurs within the basin, leaving behind seven distinct remnant terraces within the basin.

My overarching hypothesis for the study is that the Sedimentary Fill of Reynolds Creek is the key to unravelling the topographic evolution of RC. This hypothesis is not disproven, as the overall evolution of RC involves the interplay between the upper and lower basin, which is largely defined by the presence or absence of the unit within the basin. U-Th-Pb analysis was able to constrain the timing of the Sedimentary Fill of Reynolds Creek to starting at 11.127 mya, and was used to determine the mechanism for which the basin was filling overtime to be associated with the damming of the basin by the Rhyolitic lava flow of Reynolds Creek. U-Th-Pb analysis was also able to better correlate the overall distribution of sediments within the

Sedimentary Fill of Reynolds Creek. OSL analysis was used to attempt to constrain the incision history of RC, but gave insights to the overall speed that incision was occurring within the basin. RC falls in line with other volcanically dammed basins within the western Snake River Plain, and has been shown to produce signals from the damming that have persisted longer than other previously studied basins.

3.4 Figures

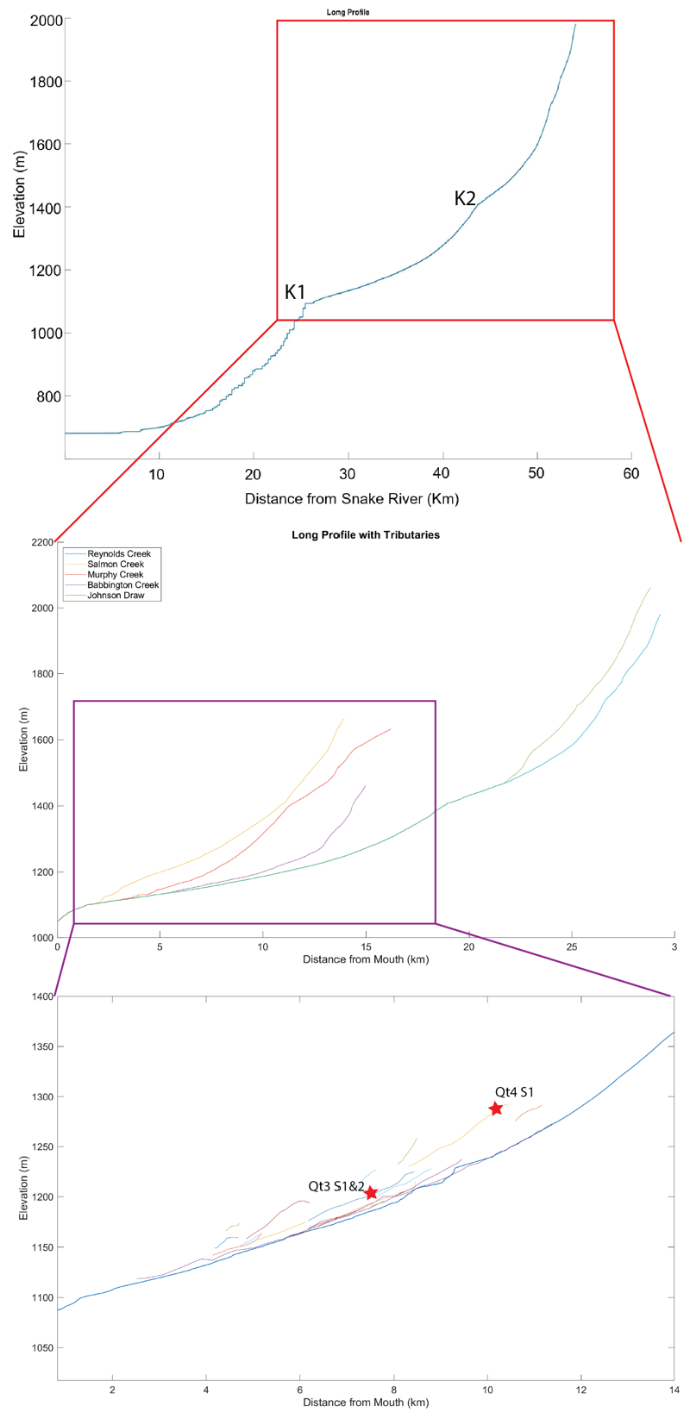

Figure 3.1: Longitudinal Profile of Reynolds Creek. Knickpoints are noted on the diagram

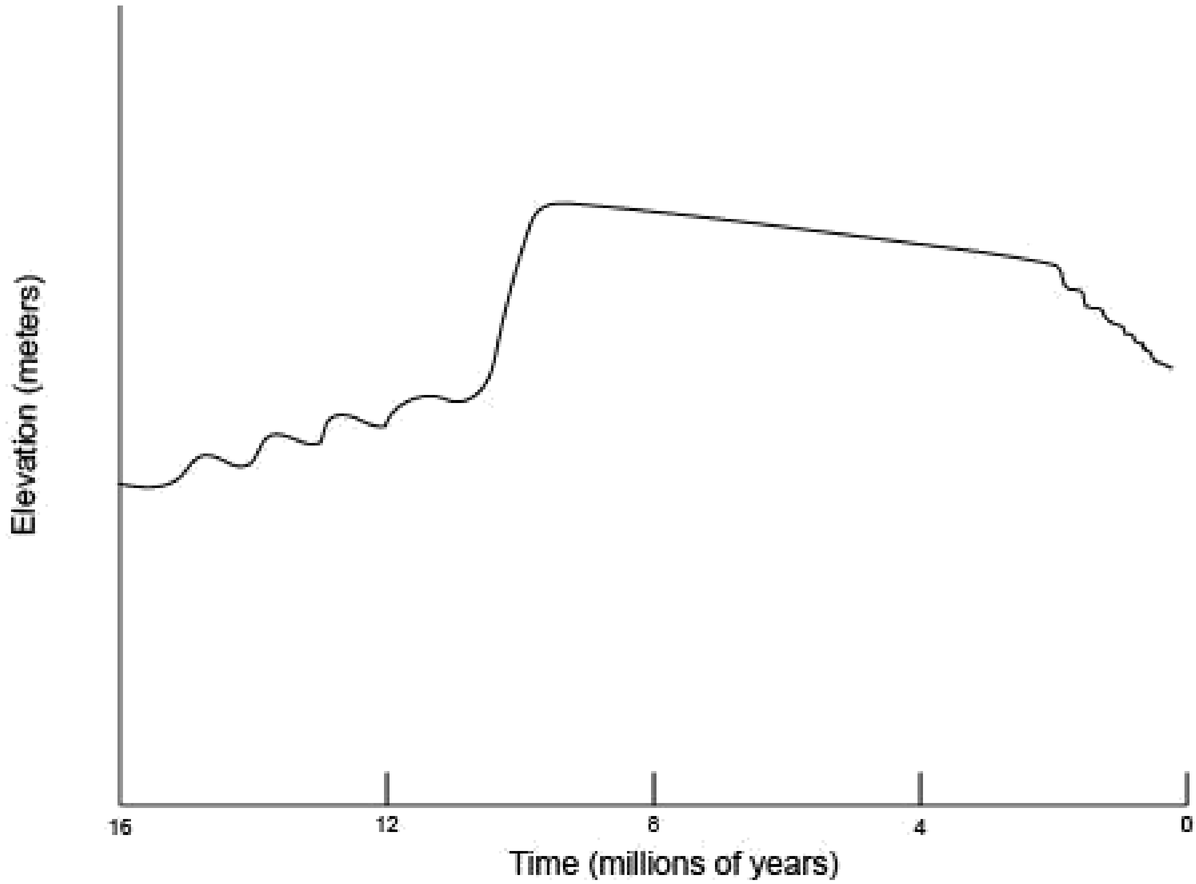

Figure 3.2: Landscape Evolution of Reynolds Creek. Notice the small jumps for volcanic emplacement and small cuts for stream incision when compared to Lacustrine fill.

3.5 References

Cheng S.P. Li C.Y. Yang G.Z. Zhou S.W., 2006, Differentiating Pleistocene tectonically driven and climate-related fluvial incision: The Sanggan River, Datong Basin, North China: Geological Magazine, v. 143, p. 393–410, doi:10.1017/S0016756806001956.

Crow, R., Karlstrom, K.E., McIntosh, W., Peters, L., Dunbar, N., 2008, History of Quaternary volcanism and lava dams in western Grand Canyon based on LiDAR analysis, 40Ar/39Ar dating, and field studies: Implications for flow stratigraphy, timing of volcanic events, and lava dams: Geosphere, v. 4, p. 183–206, doi:10.1130/GES00133.1.

Daniel, R.B., Gamble, E.E., and Cady, J.G., 1971, The relation between geomorphology and soil morphology and genesis: Advances in Agronomy, v. 23, p. 51–88

Ely, L. L., Brossy, C.C., House, P.K., Safran, E.B., O'Connor, J.E., Champion, D.E., Fenton, C.R., Bondre, N.R., Orem, C.A., and Grant, G.E., 2012, Owyhee River intracanyon lava flows: Does the river give a dam?: Geological Society of America Bulletin, vol 124, p. 1667– 1687, doi:10.1130/B30574.1

Fellows, A.W., Flerchinger, G.N., Seyfried, M.S., Lohse, K., 2017, Data for Partitioned Carbon and Energy Fluxes within the Reynolds Creek Critical Zone Observatory [Data Set]

Fenton, C.R., Webb, R.H., Cerling, T.E., Poreda, R.J., Nash, B.P., 2002, Cosmogenic He ages and geochemical discrimination of lava-dam outburst-flood deposits in western Grand Canyon, Arizona, in House, P.K., Webb, R.H., Baker, R.V., Levish, D.R., eds., Ancient Floods and Modern Hazards: Principles and Applications of Paleoflood Hydrogeology : Washington, D.C., American Geophysical Union, Water and Science Applications, v. 5, p. 191–215

Fenton, C.R., Webb, R.H., Cerling, T.E., 2006, Peak discharge of a Pleistocene lava-dam outburst flood in Grand Canyon, Arizona, USA: Quaternary Research, v. 65, no. 2, p. 324–335, doi:10.1016/j.yqres.2005.09.006.

Flerchinger, G. N., Fellows, A. W., Seyfried, M. S., Clark, P. E., Lohse, K. A., 2020, Water and carbon fluxes along an elevational gradient in a sagebrush ecosystem: Ecosystems, v. 23, p. 246-263

Jenny, H., 1941, Factors of Soil Formation: A System of Quantitative Pedology. Dover Publications, New York. 301 p.

Korup, O., Densmore, A.L., Schlunegger, F., 2010, The role of landslides in mountain range evolution: Geomorphology, v. 120, p. 77–90, doi:10.1016/j.geomorph.2009.09.017.

Liu, X., Zhao, C., Qin, Z., Peng, J., Zhu, W., Lu, Z., 2018, Multi-temporal loess landslide inventory mapping with C-, X- and L-band SAR datasets—a case study of Heifangtai loess landslides, China: Remote Sensing, v. 10, no. 1756

Pratt-Sitaula, B., Garde, M., Burbank, D.W., Oskin, M., Heimsath, A., Gabet, E., 2007, Bedload-to-suspended load ratio and rapid bedrock incision from Himalayan landslide-dam lake record: Quaternary Research, v. 68, p. 111–120, doi:10.1016/j.yqres.2007.03.005

Safran, E. B., O'Connor, J. E., Ely, L. L., House, P. K., Grant, G., Harrity, K., Croall, K., & Jones, E. 2015, Plugs or flood-makers? The unstable landslide dams of eastern Oregon: Geomorphology, v. 248, p. 237– 251. https://doi.org/10.1016/j.geomorph.2015.06.040

Seyfried, M., Lohse, K., Marks, D., Flerchinger, G., Pierson, F., Holbrook, W.S., 2018, Reynolds Creek Experimental Watershed and Critical Zone Observatory: Vadose Zone Journal, v. 17, p. 1-20

Stanbery, C.A., Pierce, J.L., Benner, S.G., Lohse, K.S. 2017, On the rocks: Quantifying storage of inorganic soil carbon on gravels and determining pedon-scale variability. Catena, v. 157, p. 436– 442

Stock, J.D., Montgomery, D.R., Collins, B.D., Dietrich, W.E., Sklar, L., 2005, Field measurements of incision rates following bedrock exposure: Implication for process controls on the long profiles of valleys cut by rivers and debris flows: Geological Society of America Bulletin, v. 117, p. 174–194, doi:10.1130/B25560.1.

APPENDIX 1: TAK code

```
% TAK Stream-Maker and Picker

% Creates a script that quickly loads in the DEM data and leads to a

% visualization in the streams. This figure will be saved and then put into

% the stream picker tool
```

```
% Clear the decks

clear, close all
```

```
%Insert TIF file for MakeStreams

[filename,pathname,filterindex]=uigetfile('*.tif','Pick a TIF file ');


% Load in the DEM data with the 'MakeStreams' tool

[DEM,FD,A,S]=MakeStreams(filename,1e6,'resample_grid',true,'no_data_exp','DEM<500
');
```

```
% Create imaging for DEM

imageschs(DEM,DEM,'colormap','gray');

hold on;

plot (S,'-c');


% Save Figure as FIG file and PDF file

savefig('ReynoldsDEM');

close
```

```
% Use auto detection scheme to find the fluvial-hillslope transition. This

% will help define the chanel heads for stream picker
```

```
[Sn, thresh_list, xd_list]=FindThreshold(DEM,FD,A,S,'auto');


% Save Figures as FIG and PDF for thresholds
savefig('Thresholdgraphs');
close
```

```
% Run SegmentPicker to obtain stream selections. In our case, we will look
% for 4 streams
[Sc1]=SegmentPicker(DEM,FD,A,S,1);
close all
[Sc2]=SegmentPicker(DEM,FD,A,S,2);
close all
[Sc3]=SegmentPicker(DEM,FD,A,S,3);
close all
[Sc4]=SegmentPicker(DEM,FD,A,S,4);
close all
```

```
% Run SegmentPlotter and save the segments as their given variable number
SegmentPlotter(1)
savefig('PickedSegment_1')
print('PickedSegment_1','-dpdf')
close all
SegmentPlotter(2)
savefig('PickedSegment_2')
print('PickedSegment_2','-dpdf')
close all
SegmentPlotter(3)
```

```
savefig('PickedSegment_3')

print('PickedSegment_3','-dpdf')

close all

SegmentPlotter(4)

savefig('PickedSegment_4')

print('PickedSegment_4','-dpdf')

close all
```

```
% Project stream portions to create an incision graph of the main stream

% network

[PROJ_OUT]=SegmentProjector(DEM,FD,A,Sc1,1);

close all

[Sproj,zpOUT,inOUT]=ProjectedIncision(DEM,A,S,Sc1,PROJ_OUT,1);

savefig('ProjectedIncisionReynolds')

print('ProjectedIncisionReynolds','-dpdf')

close all


% Create Ksn Map

[~,ksn_ms]=KsnChiBatch(DEM,FD,A,S,'ksn','file_name_prefix','ReynoldsKsn','output'

,true);

PlotKsn(DEM,FD,ksn_ms);

savefig('ReynoldsKsn');

print('ReynoldsKsn','-dpdf');

close all
```

```
function [TerracePlot] = TA(TerraceElevations,A)
%UNTITLED Summary of this function goes here
%   Detailed explanation goes here
X=A(:,2);
```

```
Y=A(:,3);
TerracePlot=plot(X,Y,'LineWidth',3);
for i=40:41
    hold on
    ind=TerraceElevations(:,1)==i;
    T=TerraceElevations(ind,:);
    X=T(:,3);
    Y=T(:,4);
    TerracePlot=plot(X,Y);
end
hold off

end
```

APPENDIX 2: U-Th-Pb Additional Data

CA-TIMS U-Pb isotopic data

	Compositional Parameters						Radiogenic Isotope Ratios								Isotopic Ages					
Sample (a)	Th/U (b)	$^{206}Pb^*$ $\times10^{-13}$ mol (c)	mol % $^{206}Pb^*$ (c)	Pb^*/Pb_c (c)	Pb_c (pg) (c)	$^{206}Pb/^{204}Pb$ (d)	$^{208}Pb/^{206}Pb$ (e)	$^{207}Pb/^{206}Pb$ (e)	% err (f)	$^{207}Pb/^{235}U$ (e)	% err (f)	$^{206}Pb/^{238}U$ (e)	% err (f)	corr. coef.	$^{207}Pb/^{206}Pb$ (g)	± (f)	$^{207}Pb/^{235}U$ (g)	± (f)	$^{206}Pb/^{238}U$ (g)	± (f)
RCC20-LM-BRP-01																				
z1	1.437	0.1023	91.38%	4	0.80	209	0.464	0.04633	2.358	0.010887	2.526	0.001704	0.220	0.779	14.6	56.6	10.99	0.28	**10.978**	**0.024**
z2	1.947	0.0403	92.19%	5	0.28	231	0.627	0.04621	2.867	0.010887	2.991	0.001709	0.210	0.612	8.8	68.9	10.99	0.33	**11.005**	**0.023**
z3	1.341	0.0960	91.66%	4	0.73	216	0.433	0.04664	2.196	0.010971	2.359	0.001706	0.214	0.773	30.9	52.5	11.08	0.26	**10.988**	**0.024**
z4	1.559	0.0363	80.60%	2	0.73	93	0.503	0.04657	6.124	0.010913	6.515	0.001700	0.542	0.738	27.1	146.6	11.02	0.71	**10.948**	**0.059**
z5	1.437	0.0759	91.38%	4	0.59	209	0.464	0.04648	2.350	0.010924	2.518	0.001704	0.220	0.779	22.7	56.3	11.03	0.28	**10.978**	**0.024**
z6	1.947	0.0243	92.19%	5	0.17	231	0.627	0.04651	2.854	0.010944	2.977	0.001706	0.210	0.611	24.4	68.4	11.05	0.33	**10.991**	**0.023**
z7	1.143	0.1101	91.66%	4	0.83	216	0.369	0.04646	2.204	0.010936	2.366	0.001707	0.214	0.773	21.7	52.8	11.04	0.26	**10.995**	**0.024**
z8	1.419	0.0705	92.03%	4	0.51	226	0.458	0.04642	2.224	0.010905	2.378	0.001704	0.212	0.743	19.4	53.3	11.01	0.26	**10.974**	**0.023**
weighted mean $^{206}Pb/^{238}U$ age = 10.986 ± 0.009 (0.01) [0.02] Ma (2s); MSWD = 0.98 (n=8) (h)																				
RCC20-LM-BRP-03																				
z1	0.769	0.0349	81.03%	1	0.68	95	0.249	0.04639	10.794	0.010276	11.010	0.001607	0.529	0.425	17.8	258.4	10.38	1.14	**10.349**	**0.055**
z2	0.871	0.0800	91.68%	4	0.60	217	0.282	0.04625	2.316	0.010279	2.474	0.001612	0.217	0.741	10.5	55.5	10.38	0.26	**10.383**	**0.022**
z3	0.836	0.1473	94.02%	5	0.78	302	0.271	0.04623	1.541	0.010263	1.659	0.001610	0.161	0.751	9.5	37.0	10.37	0.17	**10.372**	**0.017**
z4	0.789	0.0600	85.27%	2	0.86	122	0.255	0.04587	5.311	0.010181	5.561	0.001610	0.397	0.649	-9.3	127.8	10.28	0.57	**10.369**	**0.041**
z5	0.812	0.0458	87.19%	2	0.56	141	0.263	0.04659	4.741	0.010341	4.973	0.001610	0.350	0.679	28.5	113.3	10.45	0.52	**10.368**	**0.036**
z6	0.871	0.0703	91.68%	4	0.53	217	0.282	0.04625	2.316	0.010260	2.474	0.001609	0.217	0.741	10.5	55.5	10.36	0.26	**10.364**	**0.022**
z7	0.970	0.0598	90.47%	3	0.52	189	0.314	0.04544	3.260	0.010064	3.448	0.001606	0.261	0.732	-32.0	78.8	10.17	0.35	**10.347**	**0.027**
z8	2.219	0.0269	92.75%	6	0.17	249	0.715	0.04633	3.273	0.010268	3.395	0.001608	0.208	0.602	14.7	78.6	10.37	0.35	**10.355**	**0.022**
weighted mean $^{206}Pb/^{238}U$ age = 10.366 ± 0.009 (0.01) [0.02] Ma (2s); MSWD = 0.90 (n=8) (h)																				
RCC20-LM-Q																				
z1	1.295	0.0250	76.48%	1	0.64	77	0.418	0.04670	11.124	0.011009	11.499	0.001710	0.703	0.552	33.9	265.8	11.12	1.27	**11.013**	**0.077**
z2	1.502	0.0088	62.82%	1	0.43	49	0.485	0.04640	92.498	0.010911	92.688	0.001705	1.383	0.144	18.6	2216.8	11.02	10.16	**10.98**	**0.15**
z3	1.085	0.0101	71.43%	1	0.34	63	0.351	0.04659	122.449	0.010993	122.522	0.001711	0.966	0.080	28.0	2927.6	11.10	13.53	**11.02**	**0.11**
z4	1.694	0.0106	70.64%	1	0.37	61	0.546	0.04716	18.518	0.011068	18.911	0.001702	0.941	0.436	57.4	440.7	11.18	2.10	**10.96**	**0.10**
z5	1.075	0.0076	84.60%	2	0.11	117	0.347	0.04652	37.005	0.010920	37.077	0.001702	0.513	0.147	24.6	885.3	11.03	4.07	**10.965**	**0.056**
z6	1.514	0.0268	77.78%	1	0.64	81	0.489	0.04648	15.585	0.010932	15.856	0.001706	0.471	0.583	22.4	373.2	11.04	1.74	**10.988**	**0.052**
z7	1.119	0.0326	79.78%	1	0.69	89	0.362	0.04639	7.169	0.010926	7.568	0.001708	0.584	0.700	18.1	171.7	11.03	0.83	**11.002**	**0.064**
weighted mean $^{206}Pb/^{238}U$ age = 10.989 ± 0.027 (0.03) [0.03] Ma (2s); MSWD = 0.32 (n=7) (h)																				
RCC20-LM-S																				
z1	1.765	0.0367	92.84%	5	0.24	252	0.569	0.04651	3.928	0.011065	4.022	0.001725	0.206	0.476	24.4	94.1	11.17	0.45	**11.113**	**0.023**
z2	0.562	0.0476	88.60%	2	0.51	158	0.182	0.04646	3.922	0.011087	4.136	0.001731	0.312	0.699	21.4	93.8	11.20	0.46	**11.148**	**0.035**
z3	2.168	0.0271	94.02%	7	0.14	302	0.698	0.04651	3.825	0.011068	3.927	0.001726	0.220	0.483	24.1	91.7	11.18	0.44	**11.117**	**0.024**
z4	1.927	0.0303	91.84%	5	0.22	221	0.621	0.04642	3.210	0.011068	3.388	0.001729	0.234	0.774	19.7	77.0	11.18	0.38	**11.137**	**0.026**
z5	0.895	0.0406	87.19%	2	0.49	141	0.289	0.04631	9.050	0.011060	9.184	0.001732	0.361	0.386	14.0	216.9	11.17	1.02	**11.156**	**0.040**
z6	2.090	0.0522	90.42%	4	0.46	188	0.673	0.04638	2.887	0.011038	3.067	0.001726	0.254	0.731	17.2	69.3	11.15	0.34	**11.119**	**0.028**
z7	1.250	0.2039	96.70%	11	0.58	547	0.404	0.04631	0.817	0.011030	0.888	0.001728	0.103	0.708	13.6	19.6	11.14	0.10	**11.127**	**0.011**
weighted mean $^{206}Pb/^{238}U$ age = 11.127 ± 0.008 (0.01) [0.02] Ma (2s); MSWD = 1.12 (n=8) (h)																				

(a) z1, z2 etc. are labels for single zircon grains or fragments annealed and chemically abraded after Mattinson (2005); **bold** indicates results used in weighted mean calculations.
(b) Model Th/U ratio iteratively calculated from the radiogenic 208Pb/206Pb ratio and 206Pb/238U age.
(c) Pb* and Pbc represent radiogenic and common Pb, respectively; mol % $^{206}Pb^*$ with respect to radiogenic, blank and initial common Pb.
(d) Measured ratio corrected for spike and fractionation only. Fractionation calculated from the measured double spike Pb and U ratios.
(e) Corrected for fractionation, spike, and common Pb; all common Pb was assumed to be procedural blank: 206Pb/204Pb = 18.042 ± 0.61%; 207Pb/204Pb = 15.537 ± 0.52%; 208Pb/204Pb = 37.686 ± 0.63% (all uncertainties 1-sigma).
(f) Errors are 2-sigma, propagated using the algorithms of Schmitz and Schoene (2007).
(g) Calculations are based on the decay constants of Jaffey et al. (1971). 206Pb/238U and 207Pb/206Pb ages corrected for initial disequilibrium in 230Th/238U using Th/U(magma) = 2.8 ± 0.05 (1s).
(h) Age uncertainties reported as ± analytical (+tracer) [+decay constant]; MSWD = mean squared weighted deviation.

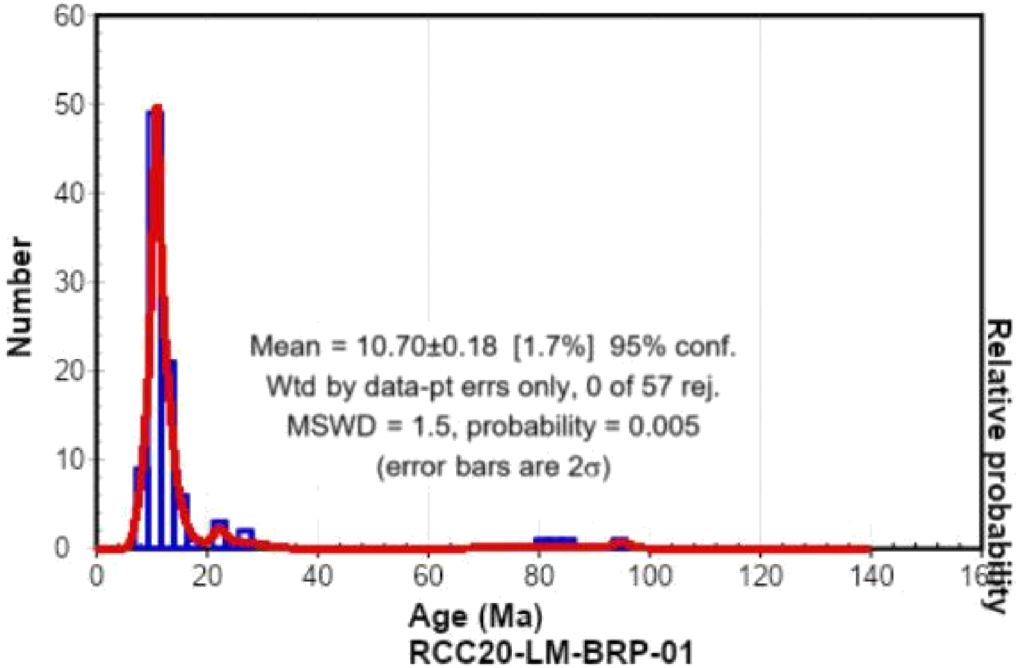
Mean = 10.70±0.18 [1.7%] 95% conf.
Wtd by data-pt errs only, 0 of 57 rej.
MSWD = 1.5, probability = 0.005
(error bars are 2σ)
Number
Relative probability
Age (Ma)
RCC20-LM-BRP-01

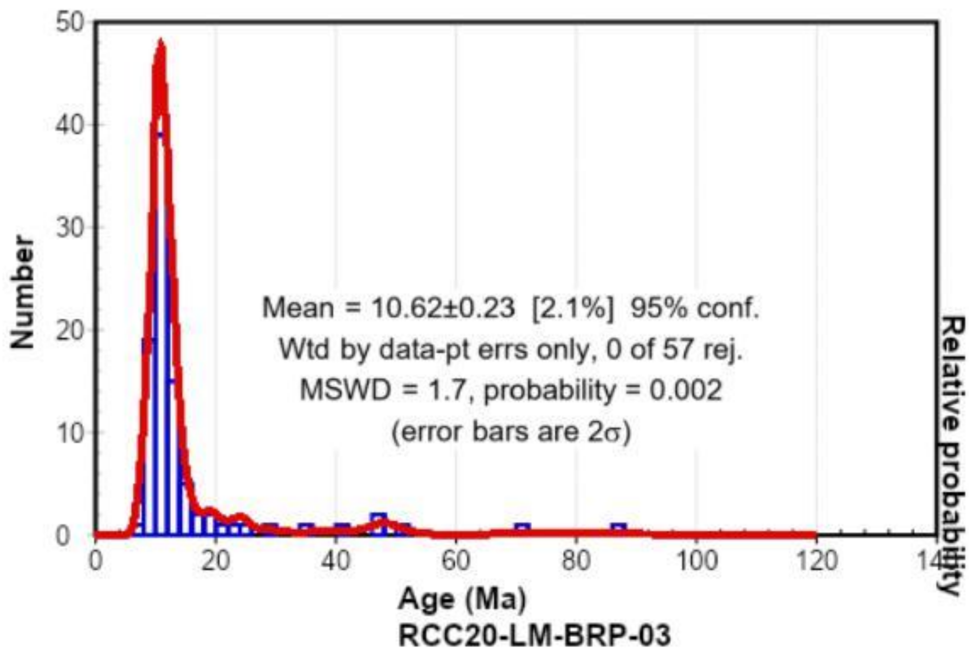
Mean = 10.62±0.23 [2.1%] 95% conf.
Wtd by data-pt errs only, 0 of 57 rej.
MSWD = 1.7, probability = 0.002
(error bars are 2σ)
Number
Relative probability
Age (Ma)
RCC20-LM-BRP-03

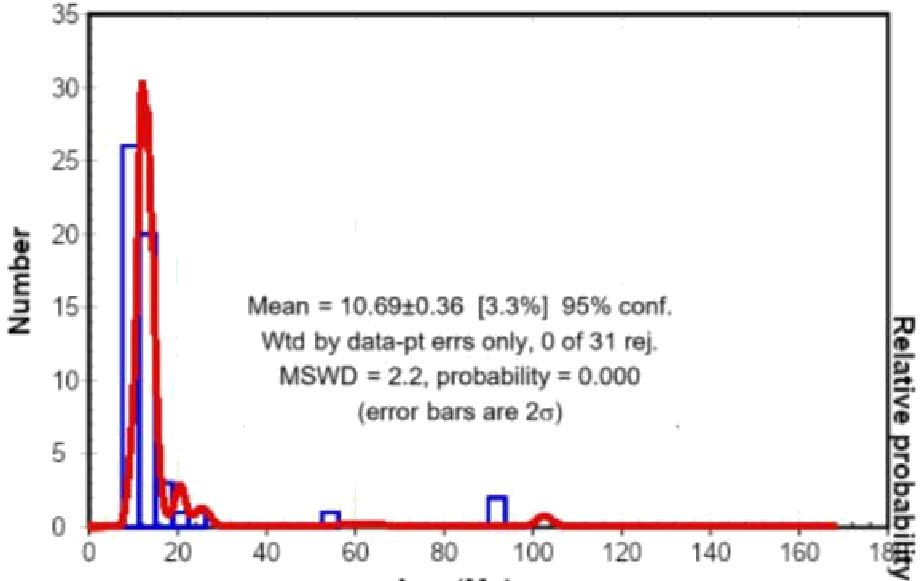

Quarry 01

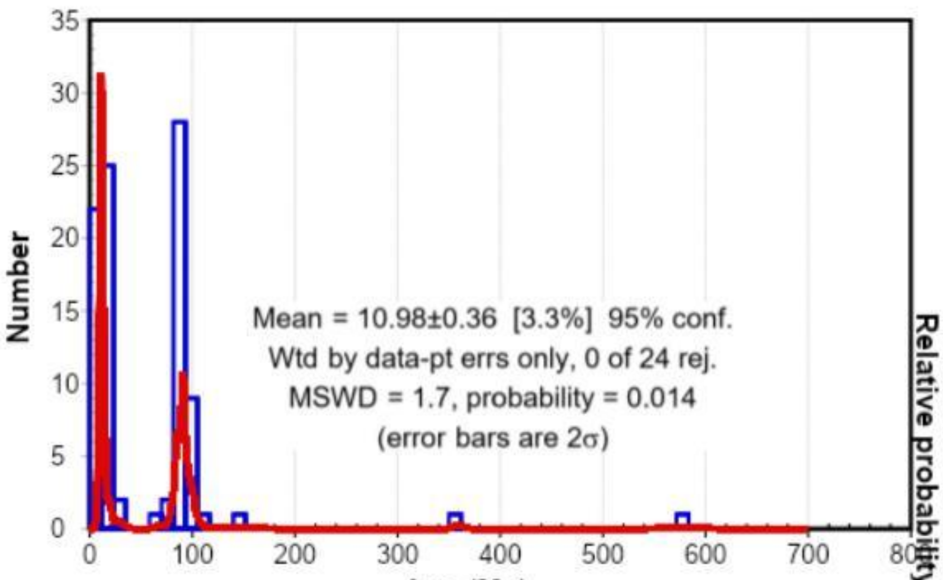

RCC20-LM-S-01

APPENDIX 3: OSL Additional Data

Final Luminescence Age Report

Table 1. Optically Stimulated Luminescence Age Information

Sample num.	USU num.	Depth (m)	Num. of aliquots[1]	Dose rate (Gy/kyr)	Equivalent Dose[2] ± 2σ (Gy)	OSL age ± 2σ (ka)
RC Pit 1-1	USU-3457	1.8-1.9	16 (32)	2.51 ± 0.11	75.42 ± 10.24	**30.02 ± 4.76**
RC Trench 1-1	USU-3458	~1	21 (31)	2.43 ± 0.10	54.16 ± 6.88	**22.30 ± 3.37**
S01RCCZOLM	USU-3464	3.5	19 (35)	2.26 ± 0.09	65.70 ± 8.23	**29.09 ± 4.35**

[1] Age analysis using the single-aliquot regenerative-dose procedure of Murray and Wintle (2000) on 1-mm small-aliquots of quartz sand (90-150 μm). Number of aliquots used in age calculation and number of aliquots analyzed in parentheses.
[2] Equivalent dose (D_E) calculated using the Central Age Model (CAM) of Galbraith and Roberts (2012).

Table 2. Dose Rate Information

Sample num.	USU num.	In-situ H_2O (%)[1]	Sub-sample fraction[2]	K (%)[3]	Rb (ppm)[3]	Th (ppm)[3]	U (ppm)[3]	Cosmic (Gy/kyr)
RC Pit 1-1	USU-3457	20.0	F: 60% M: 20% C: 20%	1.08±0.03 1.35±0.03 1.43±0.04	44.8±1.8 42.7±1.7 51.0±2.0	7.7±0.7 4.6±0.4 5.5±0.5	3.8±0.3 1.9±0.1 1.5±0.1	0.20±0.02
RC Trench 1-1	USU-3458	19.2	F: 85% M: 5% C: 10%	1.07±0.03 1.36±0.03 0.34±0.01	49.0±2.0 44.5±1.8 4.3±0.2	8.9±0.8 5.8±0.5 1.1±0.1	2.9±0.2 1.8±0.1 0.7±0.1	0.23±0.02
S01RCCZOLM	USU-3464	2.8	F: 75% M: 20% C: 5%	1.10±0.03 1.60±0.04 2.58±0.06	34.6±1.4 51.9±2.1 97.1±3.9	10.0±0.9 7.2±0.7 9.8±0.9	1.5±0.1 1.5±0.1 2.1±0.1	0.17±0.02

[1] Assumed 5.0 ± 3.0% for all samples as moisture content over burial history.
[2] Dose rate subsamples based on weighted proportions (%) of grain size subsamples: fine-F (<1.7 mm), medium-M (1.7-16 mm), coarse-C (>16 mm), and used with chemistry in gamma dose rate calculation. Fine fraction only used in beta dose rate calculation.
[3] Radioelemental concentrations determined using ICP-MS and ICP-AES techniques; dose rate is derived from concentrations by conversion factors from Guérin et al. (2011).

2. RC Trench 1-1, USU-3458

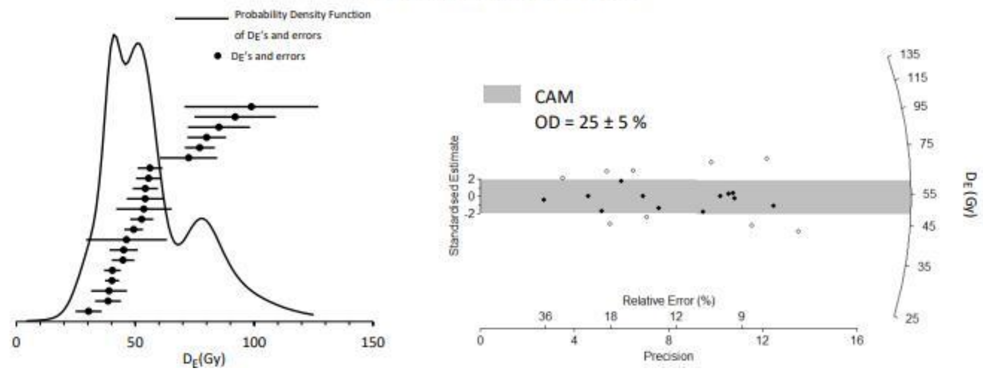

3. S01RCCZOLM, USU-3464

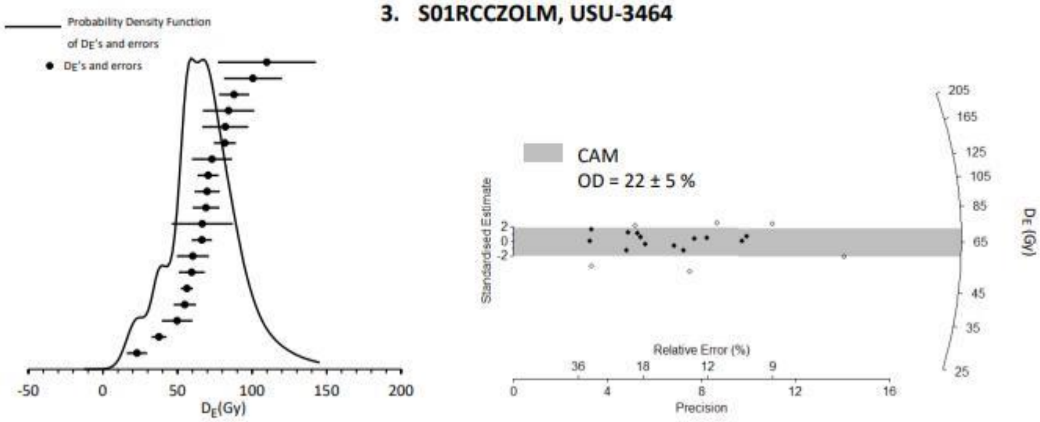

1. RC Pit 1-1, USU-3457